*Physics – Uspekhi* **56** (3) 213 – 242 (2013) 

*REVIEWS OF TOPICAL PROBLEMS* PACS numbers: **34.10.+x**, 34.50.Fa, **34.70.+e**

# Collision processes involving heavy many-electron ions interacting with neutral atoms

I Yu Tolstikhina, V P Shevelko

DOI: 10.3367/UFNe.0183.201303a.0225

## Contents



**Abstract. An overview of experimental data and theoretical computational methods is given for effective cross sections of charge exchange (electron capture) and electron loss (projectile ionization) processes involving heavy many-electron ions (like $Xe^{q+}$, $Pb^{q+}$, $W^{q+}$, $U^{q+}$) colliding with neutral atoms (H, He, N, Ne, Ar, Kr, Xe) in the $E \approx 10$ keV/u–10 GeV/u energy range, i.e., from low up to relativistic energies. These charge-changing processes can occur with a high probability, reaching $10^{-14} - 10^{-16}$ cm$^2$ cross-section values and, therefore, they play a key role in the kinetics of laboratory and astrophysical plasmas and influence the lifetimes of ion beams in accelerator facilities. Multielectron capture and loss processes are considered, as well, since their importance in the case of heavy atomic projectiles strongly increases, and a contribution to the total cross sections reaches more than 50%. An important aspect of the overview is a consideration of the influence of the inner-shell electrons of two colliding systems and a role of isotope effects in electron capture by very slow ions ($E \approx 10 - 100$ eV/u) from hydrogen isotopes H, D, and T. A short description of the corresponding computer codes is given for the calculation of cross sections of electron capture and electron loss processes for complex atoms and ions over a wide collision energy range.**

**I Yu Tolstikhina** Lebedev Physical Institute, Russian Academy of Sciences, Leninskii prosp. 53, 119991 Moscow, Russian Federation
Tel. +7 (499) 132 67 15. E-mail: inga@sci.lebedev.ru
Moscow Institute of Physics and Technology (State University), Institutskii per. 9, 141700 Dolgoprudnyi, Moscow region, Russian Federation
**V P Shevelko** Lebedev Physical Institute, Russian Academy of Sciences, Leninskii prosp. 53, 119991 Moscow, Russian Federation
Tel. +7 (499) 783 36 84. E-mail: shev@sci.lebedev.ru

Received 26 March 2012, revised 19 April 2012
*Uspekhi Fizicheskikh Nauk* **183** (3) 225 – 255 (2013)
DOI: 10.3367/UFNr.0183.201303a.0225
Translated by the authors; edited by A Radzig

## 1. Introduction

Radiation and collision processes occurring in laboratory and astrophysical plasmas are determined by the interaction of plasma particles (electrons, atoms, molecules, and ions) among themselves and with photons. These so-called *elementary* processes include excitation, ionization, recombination due to electron–atom and ion–atom collisions, and photoprocesses. Elementary processes are of interest in many branches of atomic physics and spectroscopy, plasma physics, quantum electronics, accelerator physics, and thermonuclear fusion. Moreover, determination of the relations among the characteristics of elementary processes and radiation intensities allows one to develop reliable spectroscopic and carpuscular methods for plasma diagnostics. The properties and the role of elementary processes in laboratory and astrophysical plasmas have been considered in many review articles and books [1–24].

During recent years, interest in the investigation of atomic processes involving heavy many-electron ions has strongly increased. This is related with the fast development of accelerator techniques and the employment of heavy ions in

many applications, such as thermonuclear fusion [25, 26], slowing down of heavy-ion beams in matter [27], particle beam diagnostics of laboratory plasmas [28], fragmentation of exotic nuclei [29], investigation of the interaction of laser-produced plasmas with a solid surface [30] and the generation of extreme states of matter [31], in astrophysics [32], in beam tumor therapy [33, 34], in the design of the new types of accelerators and storage rings, etc. Investigations of heavy ions accelerated up to relativistic energies are the focus of special attention in the new international FAIR project (Facility for Antiproton and Ion Research) started in 2011 at Gesellschaft für Schwerionenforschung (GSI) in Darmstadt [35].

Among different ion–atom processes, first of all one should mention those followed by a charge transfer between colliding particles. An ion colliding with an atom or molecule can reduce or increase its charge, respectively, as a result of a target-electron capture (called the *electron-capture*, *electron-transfer*, or *charge-exchange* process):

$$\mathrm{X}^{q+} + \mathrm{A} \to \mathrm{X}^{(q-k)+} + \mathrm{A}^{k+}\,, \qquad k \geqslant 1\,, \tag{1}$$

or as a result of ionization by the target atom (called the *electron-loss* process):

$$\mathrm{X}^{q+} + \mathrm{A} \to \mathrm{X}^{(q+m)+} + \sum \mathrm{A} + m\mathrm{e}^-\,, \qquad m \geqslant 1\,. \tag{2}$$

Here, $\mathrm{X}^{q+}$ denotes the projectile (impinging ion) with a charge $q$, and A is the target atom. The sum $\sum \mathrm{A}$ means that the ground-state target can be excited or ionized. For heavy ions, like $\mathrm{Xe}^{q+}$, $\mathrm{Pb}^{q+}$, $\mathrm{W}^{q+}$, and $\mathrm{U}^{q+}$, the role of multielectron processes ($k > 1$, $m > 1$) increases and their contribution to the total cross sections, i.e., summed over all $k$ and $m$, also increases reaching over 50%. Therefore, multielectron processes should be taken into account along with one-electron processes ($k = m = 1$).

As was mentioned, electron-capture and electron-loss processes play a key role in elementary processes occurring in many sources of laboratory and astrophysical plasmas, as well as in accelerator facilities. For example, electron capture in a low-temperature tokamak plasma is practically the only mechanism for creating impurity heavy ions in excited states, the radiative decay of which leads to a short wavelength radiation used for plasma diagnostics; meanwhile, electron-loss processes significantly limit the lifetimes of fast heavy ions in accelerators.

The aim of this review is to present information about the present status of charge-changing processes (electron capture and electron loss) involving heavy many-electron ions, as well as information on theoretical methods and computer codes for calculating the effective cross sections and on the cross-section scaling laws comprising the main atomic parameters: relative collision velocity, ionization potentials, nuclear and ion charges, and some others.

The main part of the review is devoted to the consideration of many-electron atoms and ions having more than one electron shell. Quite often, the presence of a large number of electrons in colliding systems leads to situations where the inner-shell electrons play a crucial and sometimes decisive role in electron-capture processes. For example, a preferential capture of the inner-shell target electrons completely defines the values and properties of electron-capture cross sections at high collision energies, while projectile ionization (electron loss) of inner-shell electrons makes the main contribution to loss cross sections at medium and high collision energies.

A system of Hartree atomic units will be used throughout: $e = m_\mathrm{e} = \hbar = 1$, where $e$ and $m_\mathrm{e}$ denote electron charge and mass, respectively, and $\hbar$ is the Plank constant.

## 2. One-electron capture processes

This section is devoted to the consideration of one-electron capture processes:

$$\mathrm{X}^{q+} + \mathrm{A} \to \mathrm{X}^{(q-1)+} + \mathrm{A}^{+}\,. \tag{3}$$

Actually, process (3) is a *reaction* with different atomic particles in the initial and final channels. Usually, one-electron capture is a dominant process; however, in the case of heavy highly charged ions ($q \gg 1$), multielectron capture becomes a very important process and makes up to 50% of the contribution to the total capture cross section because of the strong influence of a long-range Coulomb field created by the projectile (see Section 4.1).

Cross section values in reaction (3) can be very large, $10^{-14} - 10^{-16}$ cm$^2$, so these processes play a significant role in atomic physics, astrophysics, plasma physics, and accelerator physics. In particular, reaction (3) constitutes an effective mechanism of excitation transfer in plasmas [8, 10, 12] and the formation of fast beams of neutral atoms, strongly influences the charge-state distributions in passing ion beams through solid or gaseous targets [36], and plays a key role in the investigation of thermonuclear plasma confinement in tokamaks [17, 37], in the creation of an inversion population in a short-wavelength spectral range [38, 39], in astrophysics [32], in accelerator techniques [40–42], and in other areas.

In this review, the processes of *nonradiative* capture (NRC) are considered, i.e., those electron capture processes which are not related to photon radiation or absorption. The processes of *radiative* electron capture (REC), the opposite of photoionization processes, are very important in high-energy collisions of few-electron highly charged projectiles ($q \gg 1$), when the nonradiative capture processes become negligibly small (see review [43] for details).

In ion–atom collisions, the main competitive process to electron capture is electron loss — ionization of the projectile by the target atom (see Section 3). Both processes have different dependences on relative collision velocity $v$, projectile ion charge $q$, and effective charge $Z_\mathrm{eff}$ of the target atom and, therefore, the contribution of each process strongly depends on the considered energy range and atomic structures of both colliding particles. At high collision energies $E$, electron-capture (EC) $\sigma_\mathrm{EC}$ and electron-loss (EL) $\sigma_\mathrm{EL}$ cross sections exhibit the following asymptotic behavior for the target shell with a fixed charge value $Z_\mathrm{eff}$:

$$\sigma_\mathrm{EC} \sim \frac{q^5 Z_\mathrm{eff}^5}{E^{5.5}}\,, \qquad v^2 \gg I_\mathrm{P}\,, \tag{4}$$

$$\sigma_\mathrm{EL} \sim \frac{Z_\mathrm{eff}^2}{q^2 E}\,, \qquad v^2 \gg I_\mathrm{P}\,, \tag{5}$$

where $I_\mathrm{P}$ denotes the projectile binding energy. Therefore, the electron-capture cross section decreases much faster with increasing energy $E$ but depends more strongly on the charges $q$ and $Z_\mathrm{eff}$ than the electron-loss cross section.

A typical behavior of electron-capture and loss cross sections is shown in Fig. 1 by the example of collisions of

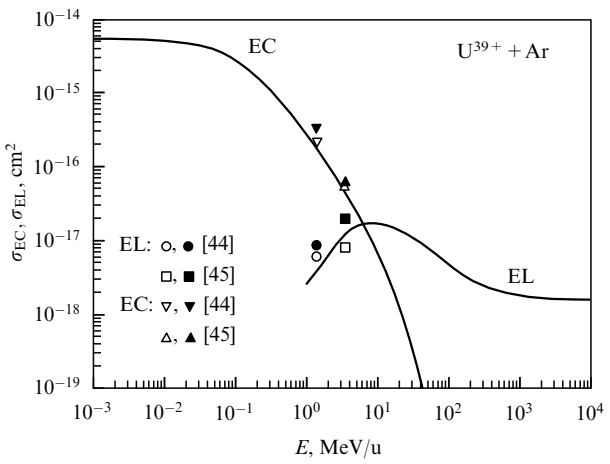


**Figure 1.** Electron-capture (EC) and electron-loss (EL) cross sections in collisions of $U^{39+}$ ions with Ar atoms as a function of collision energy. Experiment: white and black symbols — one-electron and total cross sections, respectively, from Refs [44] and [45]. Theory: solid curves — calculations by the CAPTURE, DEPOSIT, and RICODE programs (see text).

$U^{39+}$ ions (53 electrons) with Ar atoms (18 electrons). As seen from the figure, for collision energies $E < 1$ MeV/u,* the ion charge-changing cross section is mainly determined by the capture cross section, and by the loss cross section for $E > 30$ MeV/u. The energy range $E$ around 7 MeV/u, where both cross sections are of comparable size, depends on the atomic structure of both colliding particles. At relativistic energies, $E > 200$ MeV/u, the electron-loss cross section upon collision with a neutral target atom turns into a constant value but does not decrease, in accordance with law (5), because of the relativistic interaction between colliding systems (see Section 3.1.3).

In the following section, the main focus is on binary collisions when the density of the atomic or molecular target is relatively low. Upon increasing the target density, the collision frequency increases and the arising *target-density* (or gas–solid) *effects* change electron-capture and electron-loss cross section values drastically. In this case, calculations of the charge-changing cross sections differ substantially from those disregarding density effects (see Section 5).

### 2.1 Properties of one-electron capture processes. Role of capture of inner-shell electrons from the target

Electron capture reaction (3) is a complicated rearrangement process with different particles before and after collision; therefore, the theoretical investigation of these reactions constitutes a much more difficult problem than that of electron–atom collisions. At present, the cross sections for electron–atom collisions can be calculated quite accurately, with an accuracy of 10–20%, in contrast to ion–atom rearrangement collisions, where getting an accuracy within a factor of 2 is a rather tedious task. This is due to the great difficulties arising in a description of these processes: the use of different interaction potentials before and after collision event (the so-called post–prior discrepancy), the nonorthogonality of the wave functions of the system in the initial and the final channels, the Coulomb interaction between two ions in the final channel and its absence in a collision of an ion with an atom in the initial channel, and so on.

* Symbol u stands for unified atomic mass unit.

A correct formulation of the particle rearrangement problem could be made with the aid of Faddeev equations [46]. However, even in the rather simple case of charge exchange process of protons with hydrogen atoms (i.e., one electron in the field of two Coulomb centers), the Faddeev equations cannot be solved exactly; therefore, in practice, approximate methods are applied depending on the atomic parameters — relative velocity $v$ of colliding particles, their atomic structures, and the resonance defect $\Delta E_e$ of the reaction, i.e., the difference between binding energies of the active electron in both the target atom A and the resulting ion $X^{(q-1)+}$:

$$\Delta E_e = I_A(n_0 l_0) - I_X(n_1 l_1)\,,$$

where $n_0 l_0$ and $n_1 l_1$ denote the principal and the orbital quantum numbers of the target atom A and the resulting ion $X^{(q-1)+}$, respectively. We note that the resonance defect $\Delta E_e$ can be either positive or negative.

Among the different methods of calculating electron-capture cross sections, one can mention a few basic ones which give a satisfactory description of the experimental data: the close-coupling method with an atomic or molecular basis [47–50], the electron tunneling (through the Coulomb barrier) model [51], the absorbing sphere model based on the Landau–Zener theory [52], the classical overbarrier-transition model [53], the distorted-wave approximation with normalization [54, 55], relativistic treatment based on solving the two-center Dirac equation for the colliding system 'nucleus + H-like target' [56], and others. Most of the methods mentioned are described in Refs [6, 8, 11, 13, 14, 19, 21, 24]. Some methods of calculating electron-capture cross sections at low-energy collisions (for example, the adiabatic approximation, the ARSENY code) are described in detail in Section 7.

At different ion–atom collision energies, electron capture occurs as a result of different physical processes; therefore, usually two main ranges of relative collision velocity $v$ are defined: the adiabatic region with $v < v_e$, and the nonadiabatic one with $v > v_e$, where $v_e$ denotes an electron orbital velocity of the target atom. At low-energy collisions ($v < v_e$), the target bound electrons adiabatically react to the varying field of the incident ion, and, thus, a quasimolecular treatment is applied when the solution of the problem is based on the expansion of the total wave function of the system in terms of the quasimolecular wave functions at fixed internuclear distance $R$, and transitions between different states proceed as occurring between quasimolecular potential terms corresponding to localization of the active electron close to one of the nuclei. This treatment is especially effective for describing the resonance ($\Delta E_e = 0$) and quasiresonance ($\Delta E_e \approx 0$) electron capture (see, e.g., Refs [2, 11, 13, 14]).

For collision energies $E > 25$ keV/u (i.e. for $v > 1$ a.u.), when the impact (projectile) velocity is higher than the target-electron orbital velocity, $v > v_e$, the nonresonance electron capture prevails and the quasimolecular method is not valid. This is mainly related to the influence of the momentum transfer carried away by the captured electron, the so-called *translation factor* $\exp(ivr)$, which is neglected at low velocities $v$, allowing one to present the interaction matrix elements through the splitting of the corresponding molecular terms.

At relatively intermediate energies $E \sim 1-25$ keV/u, the target outer-shell electrons are captured by ions with a high probability, and due to the contribution of electron capture to a large number of excited states of the $X^{(q-1)+}$ ion, the total

cross section has a quasiconstant character, i.e., its magnitude is nearly independent of the collision energy. The quasiconstant behavior of the electron-capture cross sections in collisions of highly charged ions with neutral atoms was predicted in paper [47]. The quasiconstant magnitude of the capture cross section, which is closest to experimental data, can be estimated using the model of electron tunneling through the Coulomb barrier created by the target atom and the projectile by the formula [51]

$$\sigma(v)\left[\frac{\mathrm{cm}^2}{\mathrm{atom}}\right] \approx 10^{-15}\,\frac{q}{(I_\mathrm{T}/\mathrm{Ry})^{3/2}}\,, \quad q \geqslant 5\,, \quad v < \left(\frac{I_\mathrm{T}}{\mathrm{Ry}}\right)^{1/2}, \tag{6}$$

where $I_\mathrm{T}$ denotes the ionization potential of the target atom in Ry units (1 Ry = 13.606 eV). At intermediate collision energies, the electron capture leads to the preferential population of the $n$-states of the resulting ion $\mathrm{X}^{(q-1)+}(n)$ given by the formula ($n$ is the principal quantum number)

$$n \approx q^{3/4}\left(\frac{I_\mathrm{T}}{\mathrm{Ry}}\right)^{-1/2}. \tag{7}$$

In formula (6) and what follows, the cross sections are given in units of $\mathrm{cm}^2$/atom, i.e., they are ascribed to one target atom. This is related to the application of the *Bragg additivity rule* for *molecular* targets (see paper [57]), in accordance with which the effective cross section for the projectile interaction with a molecule is presented as a sum of the interaction cross sections for its constituent atoms. For example, the electron-capture cross section from an $\mathrm{H}_2$ target is calculated as a doubled cross section for the hydrogen atom: $\sigma(\mathrm{H}_2)$ [$\mathrm{cm}^2$] = $2\sigma(\mathrm{H})$ [$\mathrm{cm}^2$/atom]. The Bragg additivity rule is used because of the computational difficulties for molecular targets; however, this is partly justified because, at high collision energies, the main contribution to the capture (and loss) cross sections is made by the inner-shell electrons which are approximately identical in atomic and molecular targets.

At relatively high collision energies ($v > v_\mathrm{e}$), the electron-capture processes are described in terms of the first-order perturbation theory (or its modifications) on interaction of the active electron with the projectile, e.g., the distorted-wave approximation [58, 59] or the Brinkman–Kramers approximation with a multichannel normalization in the impact-parameter representation (see Section 2.2). The energy range in question covers the collision energies $E = 25$ keV/u–30 MeV/u, which is characterized by the preferential capture of inner-shell target electrons, i.e., when the electron shell structure of the target atom becomes substantial. We note that in the Brinkman–Kramers approximation, the electron-capture cross section is presented as a product of two Fourier-transforms: one for the initial wave function of the active electron, and the other for the final wave function and the electron interaction potential with the projectile ion.

The preferential role of the inner-shell target electrons is the main property of the capture reactions which makes it different from other processes in collisions of *fast* ions with atoms. With increasing energy, the capture cross section for a fixed target electron shell quickly decreases ($\sim E^{-5.5}$), in contrast to the excitation and ionization cross sections ($\sim E^{-1}$), and capture prevails for deep inner-shell electrons with the orbital electron velocity $v_\mathrm{e}$ close to the impinging ion velocity $v$: $v_\mathrm{e} \sim v$ (so-called velocity matching). Under these conditions, the contribution from the capture of outer-shell electrons becomes negligibly small compared to the case of middle and low velocities. As a result, the capture cross section summed over all target electrons decreases much more slowly than by the $E^{-5.5}$ law implemented only at very high energies, where the cross section is mainly defined by the capture of only K-shell electrons. That is why the electron-capture cross sections in collisions with light targets (H, He) decrease much faster than with heavy ones (Ne, Ar, Kr, Xe) having several electron shells.

### 2.2 Methods and computer codes for calculating electron-capture cross sections

At present, there are a few methods and computer codes for calculating electron-capture cross sections in collisions of heavy many-electron ions with atoms: CTMC (classical trajectory Monte Carlo) method for energies $E > 1$ MeV/u, CDW (continuum distorted wave) approximation for $E > 10$ MeV/u, and the normalized Brinkman–Kramers approximation (the CAPTURE code) for $E > 10$ keV/u. The accuracy of calculations using the methods mentioned is within a factor of 2.

Here, we briefly discuss these methods. The CTMC method [60] is based on the numerical solution of a system of the Hamilton classical-motion equations for all projectile and target electrons using a large number of impact parameters ($\sim 5000$) for the particle trajectories. The system consists of $6(N+2)$ nonlinear first-order equations in partial derivatives and is solved numerically for the coordinates and momenta for all $N$ electrons and two nuclei in Cartesian coordinates. Thus, for one electron ($N = 1$) moving in the Coulomb field of two nuclei a and b, the classical Hamilton equations can be written out as

$$H = \frac{p_\mathrm{a}^2}{2M_\mathrm{a}} + \frac{p_\mathrm{b}^2}{2M_\mathrm{b}} + \frac{p_\mathrm{e}^2}{2m_\mathrm{e}} + \frac{Z_\mathrm{a}Z_\mathrm{b}}{R_\mathrm{ab}} - \frac{Z_\mathrm{a}e}{R_\mathrm{ae}} - \frac{Z_\mathrm{b}e}{R_\mathrm{be}}\,, \tag{8}$$

$$\frac{\mathrm{d}C_j}{\mathrm{d}t} = \frac{\partial H}{\partial p_j}\,, \qquad \frac{\mathrm{d}p_j}{\mathrm{d}t} = -\frac{\partial H}{\partial C_j}\,, \qquad j = x, y, z\,, \tag{9}$$

where $C_j$ and $p_j$ denote coordinates and momenta of an electron and nuclei, $m_\mathrm{e}$ and $e$ are electron mass and charge, $M_\mathrm{a,b}$ and $Z_\mathrm{a,b}$ are nucleus masses and charges, and $R_\mathrm{ab}$ is the distance between the nuclei. From Eqn (9) one has 18 bound first-order differential equations for coordinate and momentum evolutions of all particles.

The use of the CTMC method is quite complicated, because many electrons and atomic trajectories should be taken into account to get enough statistics for the calculated electron-loss and electron-capture cross sections (see Section 3.2.1). The CTMC method is applied for the intermediate collision energy range, where molecular effects can be neglected. We note that because of the computational difficulties mentioned, the number of publications on CTMC electron-capture cross sections involving heavy ions is quite limited, even for one-electron capture data (see, e.g., Refs [61–63]).

The CDW method [55, 58, 59] is based on the modified Born (distorted-wave) approximation for the calculation of one-electron capture cross sections in collisions of many-electron ions with atoms at sufficiently high energies, $E > 10$ MeV/u. The method utilizes the Clementi–Roetti functions as the bound-state wave functions, and the Coulomb functions for continuum states. One of the advantages of the method is the possibility of calculating the partial capture cross sections with transitions to specific

*nl* states of the resulting $X^{(q-1)+}$ ion with different orbital momenta *l*.

The eikonal approximation [64] is intended for computing one-electron capture cross sections and is based on the semiclassical approximation with three main assumptions: a straight ion trajectory, hydrogen-like bound electron wave functions, and distorted wave functions in the final channel described by the eikonal phase factor. At present, this approximation is used very rarely (see, e.g., paper [61]).

The CAPTURE code [65] is meant for calculating probabilities and cross sections of one-electron capture and is built around the Brinkman–Kramers approximation (the Born approximation without account for the internuclear interaction) normalized in the impact parameter ($b$) representation. In the Brinkman–Kramers approximation, the electron capture probability in the Born approximation has the form (see monograph [1])

$$P(b,v) = \left|a(b,v)\right|^2 , \qquad a(b,v) = \int_{-\infty}^{\infty} \mathrm{d}t \, \exp\left(-\mathrm{i}\Delta E_\mathrm{e} t\right) \times \int \mathrm{d}\mathbf{r} \, \varphi_\mathrm{X}^*(\mathbf{r}_2) \, V \varphi_\mathrm{A}(\mathbf{r}_1) \exp\left(\mathrm{i}\mathbf{v}\mathbf{r}\right) = \frac{1}{(2\pi)^2 v} \int_P \mathrm{d}\mathbf{k} \, \Phi_\mathrm{X}^*(\mathbf{k}) \, \Phi_\mathrm{A}(\mathbf{a}) \exp\left(\mathrm{i}\mathbf{k}\mathbf{b}\right) . \tag{10}$$

Here, $\mathbf{r} = (\mathbf{r}_1 + \mathbf{r}_2)/2$, $\Delta E_\mathrm{e}$ is the resonance defect of the reaction, $V$ denotes the interaction potential of the active electron with the resulting ion $X^{q+}$, and subscripts A and X refer to the wave functions of the target atom A and the ion $X^{(q-1)+}$, respectively. The integration in formula (10) is performed over the plane $P$ described by the equation

$$\mathbf{k}\mathbf{v} - \Delta E_\mathrm{e} - \frac{v^2}{2} = 0 .$$

The functions $\Phi$ are the Fourier transforms of the wave function $\varphi_\mathrm{X}$ and the product $V\varphi_\mathrm{A}$:

$$\Phi_\mathrm{X}^*(\mathbf{k}) = \int \mathrm{d}\mathbf{r} \, \varphi_\mathrm{X}^*(\mathbf{r}) \exp\left(\mathrm{i}\mathbf{k}\mathbf{r}\right) ,$$

$$\Phi_\mathrm{A}(\mathbf{a}) = \int \mathrm{d}\mathbf{r} \, V(\mathbf{r}) \, \varphi_\mathrm{A}(\mathbf{r}) \exp\left(-\mathrm{i}\mathbf{a}\mathbf{r}\right) ,$$

$$\mathbf{k} - \mathbf{a} = \mathbf{v} , \quad k^2 - a^2 = 2\Delta E_\mathrm{e} .$$

The integral (10) over the Fourier transform product constitutes a quantum-mechanical electron-capture amplitude in the Brinkman–Kramers approximation for the straight line trajectory.

The CAPTURE code calculates the normalized electron-capture probabilities $P^{(\mathrm{norm})}(b,v)$ as functions of the impact parameter $b$ and collision velocity $v$, as well as the electron-capture cross sections corresponding to the $n$-states of the resulting ion $X^{(q-1)+}(n)$ and the total (summed over $n$) cross sections $\sigma_\mathrm{tot}(v)$:

$$\sigma_\mathrm{tot}(v) = \sum_{n=n_0}^{n=n_\mathrm{cut}} \sigma_n(v) , \qquad \sigma_n(v) \equiv \sum_s \sigma_{sn}(v) ,$$

$$\sigma_{sn}(v) = 2\pi \int_0^\infty P_{sn}^{(\mathrm{norm})}(b,v) b \, \mathrm{d}b , \tag{11}$$

$$P_{sn}^{(\mathrm{norm})}(b,v) = \frac{P_{sn}(b,v)}{1 + \sum_{n'=n_0}^{n_\mathrm{max}} P_{sn'}(b,v)} .$$

Here, $P_{sn}(b,v)$ denotes the not normalized Brinkman–Kramers probability of a capture from the target electron shell $s$ into the $n$-state of the $X^{(q-1)+}(n)$ ion, and $n_\mathrm{max}$ is the maximum principal quantum number accounted for in the code. The parameter $n_\mathrm{cut}$ depends on the target density: $n_\mathrm{cut}$ is large for low-density targets (a rarefied gas) and strongly decreases in the case of high-density targets (foils) due to the influence of target-density effects (see Section 5).

In the CAPTURE code for the active electron carrying out the transition, the hydrogen-like wave functions are employed in the initial (the target atom) and final [$X^{(q-1)+}(n)$ ion] states, with the effective charge accounting for the electron screening. The main advantage of the CAPTURE code is the use of the normalized capture probabilities which are always less than unity: $P_{sn}^{(\mathrm{norm})}(b,v) < 1$. This circumstance allows one to perform calculations over a wide energy range: from a few dozen keV/u to a few dozen MeV/u.

The low-energy limit of applicability of the normalized Brinkman–Kramers approximation depends on the atomic structure of colliding particles. The CAPTURE code leaves room for accounting the final states with a large number $n$ (up to $n_\mathrm{max} \approx 500$), which are required in calculations of the normalized capture cross sections for highly charged ions, $q \gg 1$, impinging on atoms.

To estimate one-electron capture cross sections, a semiempirical formula [66] based on experimental data is often utilized:

$$\sigma_\mathrm{Sch} \left[\frac{\mathrm{cm}^2}{\mathrm{atom}}\right] = \frac{1.1 \times 10^{-8}}{\tilde{E}^{4.8}} \frac{q^{0.5}}{Z_\mathrm{T}^{1.8}} \left(1 - \exp\left(-0.037\tilde{E}^{2.2}\right)\right) \times \left(1 - \exp\left(-2.44 \times 10^{-5}\tilde{E}^{2.6}\right)\right) , \tag{12}$$

$$\tilde{E} = \frac{E}{Z_\mathrm{T}^{1.25} q^{0.7}} , \qquad q \geqslant 3 , \qquad \tilde{E} \geqslant 10 , \tag{13}$$

where $Z_\mathrm{T}$ is the target nuclear charge, and $E$ [keV/u] is the energy of the projectile. Formulas (12) and (13) reflect the scaling law for the electron-capture cross sections as a function of collision energy, projectile charge, and target nuclear charge, and are widely used for estimating the cross sections with an accuracy up to a factor of 2.

In the limits of low and high energies, semiempirical formula (12) exhibits the following asymptotic behavior:

$$\sigma_\mathrm{Sch}(E \to 0) \left[\frac{\mathrm{cm}^2}{\mathrm{atom}}\right] \approx 10^{-14} \frac{q^{0.5}}{Z_\mathrm{T}^{1.8}} , \tag{14}$$

$$\sigma_\mathrm{Sch}(E \to \infty) \left[\frac{\mathrm{cm}^2}{\mathrm{atom}}\right] \approx 1.1 \times 10^{-8} \frac{q^{3.86} Z_\mathrm{T}^{4.2}}{E^{4.8}} . \tag{15}$$

It should be noted that formula (6) describes the dependences on the atomic parameters more correctly than formula (14); therefore, estimate (14) should be applied with caution, because it can overestimate or underestimate the capture cross sections at low collision energies.

Typical examples of electron-capture cross sections in collisions of many-electron ions with atomic and molecular targets are presented in Figs 2 and 3. Capture cross sections in $Ge^{31+} + Ne$ and $Xe^{18+} + N_2$ collisions are given in Fig. 2, where experimental data are compared with results obtained with the CTMC, eikonal, and CDW approximations, as well as using the CAPTURE code and semiempirical formula (12). As is seen from the figure, in the case of collisions between

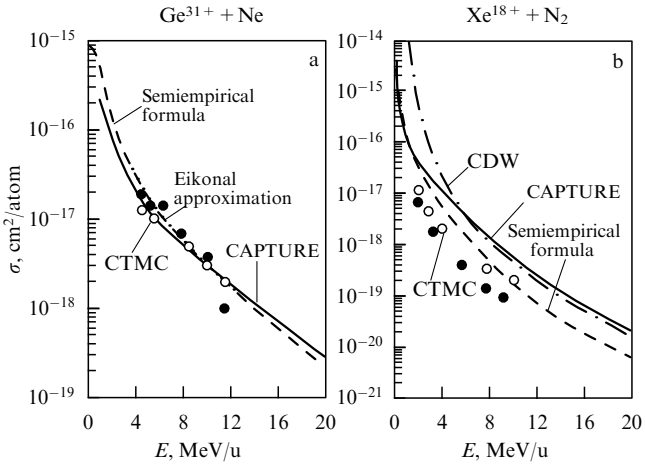


**Figure 2.** One-electron-capture cross sections in collisions of H-like $Ge^{31+}$ ions with Ne atoms (a), and $Xe^{18+}$ ions with $N_2$ molecules (b), as a function of the projectile energy. Experiment: black circles [61] (a), [68] (b); dashed curves — semiempirical formula (12). Theory: white circles — CTMC results [61] (a), [68] (b); dotted curve (a) — eikonal approximation [61]; dot-and-dash curve (b) — CDW results [67]; solid curves — CAPTURE code [67].

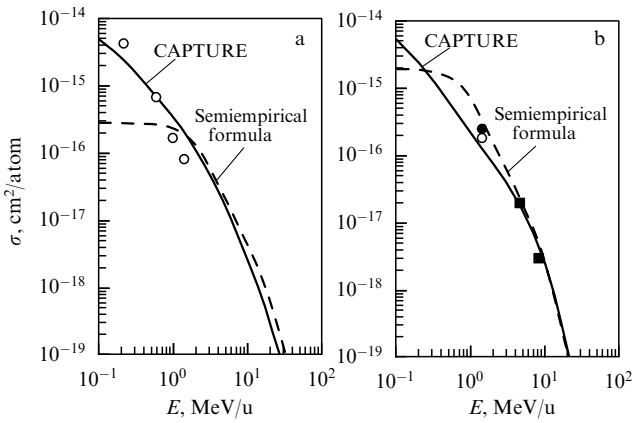


**Figure 3.** Electron-capture cross sections in collisions of $Pb^{25+}$ ions with Ar atoms (a), and $Pb^{39+}$ ions with $N_2$ molecules (b), as a function of the projectile energy. Experiment: (a) white circles — [44], (b) white and black circles — one-electron and total capture cross sections [44], black squares — [69]; dashed curves — semiempirical formula (12). Theory: solid curves — CAPTURE code [67].

H-like $Ge^{31+}$ ions and Ne atoms, all theoretical data are in rather good agreement with experiment. However, a quite large disagreement is observed for collisions of $Xe^{18+}$ ions with an $N_2$ target: the results utilizing the CDW and CAPTURE codes overestimate experimental data 5–6-fold, and CTMC results, although showing a better agreement, also overestimate the experimental data about 3-fold at high energies.

Electron-capture cross sections in collisions of lead ions with Ar and $N_2$ targets are displayed in Fig. 3. For collision energies $E > 3$ MeV/u, experimental data are in rather good agreement with the semiempirical formula (12) and results obtained with the CAPTURE code; at lower energies, formula (12) is not valid due to the energy limitation given in formula (13).

From an analysis of experimental and theoretical data on electron capture by heavy many-electron ions from atoms, it is possible to make the following conclusions:

(1) The existing computer codes describe available experimental data with an accuracy up to a factor of 2 over a wide energy range — from tens of keV/u to tens of MeV/u. Nonetheless, disagreement between theory and experiment in some cases is more than 10-fold, e.g., in $U^{28+} + Ar$ and $N_2$ collisions. The reasons for this discrepancy, at least for atomic targets, are not yet clear. It is worth noting that reactions (1) and (3) represent a particular case of more general charge-changing reactions, so-called *transfer ionization*, in which charge exchange occurs simultaneously with ionization of the target atom:

$$X^{q+} + A \to X^{(q-k)+} + A^{i+} + (i-k)e^- . \qquad (16)$$

Therefore, reactions (1) and (3) are a special case of reaction (16) at $i = k$. Usually, the measured value in experiments is a number of the resulting $X^{(q-k)+}$ ions, whereas the corrected cross-section data can be obtained by simultaneous measurement of both charged particles, i.e., scattered projectiles and target ions using the *coincidence technique*. However, the amount of experimental data obtained with the help of the coincidence technique is very limited; therefore, a corrected comparison of calculated data with experimental cross sections should be performed taking into account the possible influence of reaction (16) on the measured cross sections (see paper [70]).

(2) The disagreement between the theoretical and experimental electron capture data for molecular targets can be related to the unrightful use of the Bragg additivity rule (see Section 2.1) because, strictly speaking, the impinging ion interaction with a molecular target cannot be presented as a sum of ion interactions with atoms composing the molecule. This question was discussed in Ref. [71], and it was found that the electron-capture cross section ratio for molecular and atomic hydrogen is not equal to 2, $\sigma(H_2)/\sigma(H) \neq 2$, but, upon increasing the collision energy, the ratio nonmonotonically increases from 0.8 to 4.0. Thus, the question of the use of the Bragg additivity rule for molecular targets needs further consideration.

(3) As for many-electron capture processes involving heavy highly charged ions (see Section 4.1), it was found experimentally that the total capture cross section increases with increasing projectile charge, but the general cross-section dependences on the energy and atomic structures of the target and projectile have not been investigated experimentally and theoretically in detail so far (see, e.g., Refs [44, 45]).

## 3. Electron loss processes (projectile ionization)

Electron-loss processes (2) are competitive with the electron capture reactions considered in Section 2, and, therefore, they also play a key role in atomic processes occurring in laboratory and astrophysical plasmas and accelerator facilities.

Experimentally and theoretically, electron loss processes with heavy ions and atoms are studied in more detail than the capture processes, including multielectron loss processes with $m > 1$. Electron-loss cross sections are quite large at low and intermediate collision energies even for the ionization of highly charged projectiles, in particular, by heavy many-electron targets (see Section 4.2).

### 3.1 Born approximation

At present, a few approaches are applied for calculating the one-electron-loss cross sections in collisions of fast ions with neutral atoms: the Born approximation [72], the sudden-perturbation method [73], the CTMC method [60], and the classical energy-deposition model [74].

In the first-order of the time-dependent perturbation theory, the electron-loss probability in the impact-parameter representation is defined by the following expression (see paper [72]):

$$P(b,v) = \left|a(b,v)\right|^2 ,$$

$$a(b,v) = \int_{-\infty}^{\infty} \mathrm{d}t \, \exp\left(-\mathrm{i}\Delta E_{\mathrm{e}} t\right) \times \left\langle \varphi_{\mathrm{T}}^{(\mathrm{f})}(\mathbf{r}_j)\, \varphi_{\mathrm{X}^+}(\mathbf{r}_1) \middle| V \middle| \varphi_{\mathrm{T}}^{(\mathrm{i})}(\mathbf{r}_j)\, \varphi_{\mathrm{X}}(\mathbf{r}) \right\rangle ,$$

$$V = \frac{Z_{\mathrm{T}}}{|\mathbf{R}+\mathbf{r}|} - \sum_{j=1}^{N_{\mathrm{T}}} \frac{1}{|\mathbf{R}+\mathbf{r}-\mathbf{r}_j|} ,$$

$$\Delta E_{\mathrm{e}} = I_{\mathrm{P}} + \varepsilon + \Delta E_{\mathrm{if}} ,$$

where $\varphi_{\mathrm{T}}^{(\mathrm{i,f})}$ and $\varphi_{\mathrm{X,X^+}}$ denote the wave functions of the target atom and the impinging ion before and after collision, respectively, $V$ is the Coulomb interaction potential between the active electron and the target nucleus and electrons, $I_{\mathrm{P}}$ is the binding energy of the projectile, $R$ is the distance between nuclei, $\varepsilon$ is the kinetic energy of the ejected electron, and $\Delta E_{\mathrm{if}}$, $Z_{\mathrm{T}}$, and $N_{\mathrm{T}}$ denote the excitation energy, the nuclear charge, and the total number of electrons of the target atom.

After some transformations, the electron-loss cross section of an ion by a structured particle is presented as an integral of the product of the form factors of colliding particles over the momentum transfer $K$ (see Ref. [75]):

$$\sigma_{\mathrm{EL}}(v) = \frac{8\pi}{v^2} \sum_{nl} N_{nl} \sum_{\lambda} \int_0^{\infty} \mathrm{d}\varepsilon \int_{K_0}^{\infty} \frac{\mathrm{d}K}{K^3}\, F_{\mathrm{T}}^2(Z_{\mathrm{T}}, N_{\mathrm{T}}, K)\, F_{nl}^2(\varepsilon, \lambda, K) , \tag{17}$$

$$K_0 = \frac{I_{nl}+\varepsilon}{v} , \qquad F_{nl} = \left\langle \varepsilon\lambda \middle| \exp\left(\mathrm{i}\mathbf{Kr}\right) \middle| nl \right\rangle , \tag{18}$$

where $v$ is the ion velocity, $I_{nl}$ is the electron binding energy in the $nl$-shell of the projectile, $|nl\rangle$ and $|\varepsilon\lambda\rangle$ are the wave functions of the bound and continuum states of the active electron, respectively, $\lambda$ is the orbital angular momentum of the ejected electron, and $F_{nl}$ is the form factor of the projectile. The sum over $nl$ in expression (17) means summation over all electron shells of the projectile, and $n$ and $l$ are the principal and orbital quantum numbers of the electronic shell with $N_{nl}$ equivalent electrons.

In deriving formula (17), an additional assumption was made, namely the so-called closure approximation: $\Delta E_{\mathrm{if}} \ll I_{\mathrm{P}} + \varepsilon$, which makes the lower integration limit $K_0$ independent of the excitation energy $\Delta E_{\mathrm{if}}$ and significantly simplifies numerical calculations. Actually, the dependence $K_0$ on $\Delta E_{\mathrm{if}}$ is important only for light target atoms like H and He and leads to increasing the electron-loss cross sections by a factor of about 2 (see, e.g., monograph [21]).

The target effective charge $F_{\mathrm{T}}$ depends on the momentum transfer $K$, the target nuclear charge and the number of electrons, and has the form

$$\left|F_{\mathrm{T}}(K)\right|^2 = \left[Z_{\mathrm{T}} - \sum_{j=1}^{N_{\mathrm{T}}} \left\langle j \middle| \exp\left(\mathrm{i}\mathbf{Kr}\right) \middle| j \right\rangle\right]^2 + \left[N_{\mathrm{T}} - \sum_{j=1}^{N_{\mathrm{T}}} \left|\left\langle j \middle| \exp\left(\mathrm{i}\mathbf{Kr}\right) \middle| j \right\rangle\right|^2\right] ,$$

where $|j\rangle$ denote the radial wave functions of the target electrons. It should be noticed that the expression for the target effective charge $F_{\mathrm{T}}(K)$ was obtained using the completeness of the target wave functions and includes only the diagonal matrix elements. The formula for the electron-loss cross section of atoms and ions by a bare nucleus with the charge $Z_{\mathrm{T}}$ has a form similar to formulas (17) and (18) with $F_{\mathrm{T}}(K) \equiv Z_{\mathrm{T}}$.

The calculation of the electron-loss cross sections even in a simplified Born approximation is quite complicated because of the necessity of calculating a large number of the radial wave functions for the bound (projectile shells) and continuum (set of $\lambda$) states, as well as integrating over energies $\varepsilon$ of the ejected electron.

The effective charge $F_{\mathrm{T}}$ exhibits the following asymptotic behavior for the momentum transfer $K$:

$$F_{\mathrm{T}}^2(K) \to (Z_{\mathrm{T}} - N_{\mathrm{T}})^2 , \qquad K \to 0 , \tag{19}$$

$$F_{\mathrm{T}}^2(K) \to Z_{\mathrm{T}}^2 + N_{\mathrm{T}} , \qquad K \to \infty . \tag{20}$$

Formulas (19) and (20) reflect the influence of screening and antiscreening effects of the target electrons on the cross sections at low and high collision velocities, respectively. The asymptotics (20) stands for the limiting case of very large projectile velocities when the target nucleus and electrons can be treated at rest in the coordinate system associated with the projectile. Then, the cross section can be approximately presented by the Born formula written down through the ion ionization cross sections by electron ($\sigma_{\mathrm{e}}$) and proton ($\sigma_{\mathrm{p}}$) impacts in the form

$$\sigma_{\mathrm{EL}} \approx Z_{\mathrm{T}}^2 \sigma_{\mathrm{p}}(v) + N_{\mathrm{T}} \sigma_{\mathrm{e}}(v) , \qquad v \gg I_{\mathrm{P}}^{1/2} , \tag{21}$$

where $I_{\mathrm{P}}$ is the projectile ionization potential. As follows from last formula, the electron-loss cross section of fast ions colliding with neutral atoms is proportional to the scaling factor $Z_{\mathrm{T}}^2 + Z_{\mathrm{T}}$, i.e., the heavier the target atom, the larger the electron-loss cross section. Numerical calculations show that the dependence of the loss cross sections for heavy ions on $Z_{\mathrm{T}}$ is a little weaker than given by $Z_{\mathrm{T}}^2 + Z_{\mathrm{T}}$, viz. $\sigma_{\mathrm{EL}} \sim Z_{\mathrm{T}}^{1.8}$ due to the screening effects for the target electrons (see Section 3.1.3 and Ref. [76]).

For *many-electron* heavy projectiles, the calculation of the electron-loss cross sections by formula (17) requires accounting for the contribution of electron ionization from a large number of the target shells (about 5–10 shells) independently of the target particle — an electron, proton, or complex atom. For example, to calculate electron-loss cross sections of $\mathrm{U}^{28+}$ ions having 64 electrons, it is necessary to account for ionization from 9 electron shells of the uranium ion — from the $3s^2$ inner shell up to the $5p^2$ outer shell. The binding energies and ionization potentials for heavy atoms and ions, required for numerical calculations, can be found in data compilations [77–80].

At high collision velocities, the Born electron-loss cross sections have the following asymptotic form:

$$E \to \infty\,, \qquad v \to \infty\,, \qquad \sigma_{\rm EL} \to \frac{\ln v}{v^2}\,. \tag{22}$$

**3.1.1 LOSS and LOSS-R computer codes.** Calculations of the one-electron-loss cross sections in the nonrelativistic Born approximation using formulas (17), (18) are realized in the LOSS code described in paper [75]. There, the radial wave functions of the active electron for the bound ($|nl\rangle$) and continuum ($|\varepsilon l\rangle$) states are calculated by numerical solution of the Schrödinger equation with the effective potential of the atomic core, while the nodeless analytical Slater functions are used for the target-electron wave functions. The accuracy of calculations of the electron-loss cross sections by the LOSS code is about 30% above the cross-section maximum.

Examples of electron-loss cross sections for heavy ions colliding with atoms and molecules are displayed in Fig. 4 as functions of collision energy; furthermore, experimental data are compared here with the results of the LOSS code. In the case of an $N_2$ target, the Bragg additivity rule was applied, similarly to the calculation of the electron-capture cross sections.

In recent years, interest in the behavior of electron-loss cross sections of heavy many-electron ions colliding with neutral atoms at relativistic energies $E > 200$ MeV/u has grown significantly. This is related to a purely theoretical interest, as well as to experimental investigations started in 2011 by the International FAIR project [35], in the framework of which the acceleration of $U^{28+}$ ions is planned up to 10 GeV/u. We note that the measurement data on and calculations of electron-loss cross sections for such ions in the relativistic energy range are very scarce (see Refs [76, 84, 85]).

Properties of relativistic electron-loss cross sections are investigated in more detail for H- and He-like projectiles, i.e., ions with one and two electrons (see Refs [86–90]). The main difficulty arising in calculations of such cross sections reduces to finding the ionization matrix elements in the relativistic Born approximation [86]:

$$M_{\rm EL} = \left\langle f \middle| (1 - \beta\alpha_z) \exp\left(\mathrm{i}\mathbf{Kr}\right) \middle| i \right\rangle, \tag{23}$$

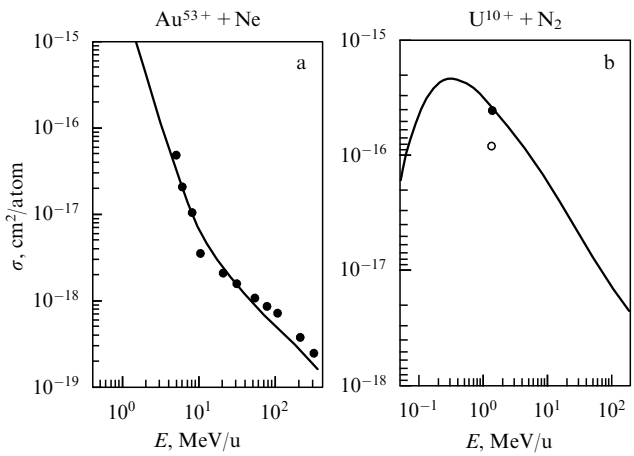


**Figure 4.** One-electron loss cross sections in collisions of $Au^{53+}$ ions (26 electrons) and $U^{10+}$ ions (82 electrons) with Ne atoms and $N_2$ molecules, respectively, as a function of the projectile energy. Experiment: black circles — [81] (a), [82] (b); white circle — [83] (b). Theory: solid curves — result of the LOSS code.

where $v$ is the projectile velocity, $\beta = v/c$ is the relativistic factor, $c$ is the speed of light, $\alpha_z$ denotes the $z$-component of the Dirac matrix $\boldsymbol{\alpha}$, and $|i\rangle$ and $|f\rangle$ are the wave functions of the system before and after collision event.

The first term in expression (23) exhibits the contribution to the matrix element made by the interaction of the projectile with the scalar potential of the neutral target atom, and corresponds to the usual nonrelativistic Born approximation (17), (18). The second term, often called *magnetic interaction*, gives the contribution from the vector potential of the target. Calculation of the second term is usually a quite complicated problem which was realized mainly for ionization of H- and He-like ions from $n$-states with $n = 1-6$ [89, 90].

The contribution of the second (relativistic) term to the matrix element (23) can be estimated as follows:

$$\beta\alpha_z \sim \frac{v}{c}\,\frac{\langle p_{\rm e}\rangle}{m_{\rm e}c} \sim \frac{v}{c}\,\frac{v_{\rm e}}{c}\,, \tag{24}$$

where $m_{\rm e}$, $v_{\rm e}$, and $\langle p_{\rm e}\rangle$ denote the rest mass, orbital velocity, and momentum matrix element of the projectile electron, respectively. As is seen from the last formula, the influence of the magnetic interaction is maximal ($\beta\alpha_z \sim 1$) when the projectile velocity $v$ and electron orbital velocity $v_{\rm e}$ are close to the speed of light; there are some other situations where the magnetic interaction makes a considerable contribution, for example, when the ion velocity is small ($v \ll c$), but ionization takes place with a small momentum transfer $K$ (see monograph [88]).

To investigate the properties and to perform numerical calculations of the electron-loss cross sections for heavy ions, a package of computer codes was created at the Lebedev Physical Institute, RAS (Moscow), including: LOSS-R (Relativistic LOSS) [91], HERION (High Energy Relativistic IONization) [92], and RICODE (Relativistic Ionization CODE) [76]. Among all codes, the RICODE program has the highest accuracy for calculating one-electron loss cross sections within a wide energy range covering relativistic energies.

The LOSS-R code is based on the same equations (17), (18) as the LOSS code but with two differences in relative velocity and a minimum momentum transfer $K_0$:

$$v \to \beta c\,, \qquad K_0 \to \frac{I_{nl} + \varepsilon}{\gamma v}\,, \qquad \gamma = \frac{1}{\sqrt{1-\beta^2}}\,, \tag{25}$$

i.e., minimum momentum transfer $K_0$ is $\gamma$ times smaller than the nonrelativistic one (18), where $\gamma$ is the relativistic factor. At relativistic energies, the LOSS-R code provides the correct asymptotic cross-section behavior [cf. Eqn (22)]:

$$E \to \infty\,, \quad v \to c\,, \quad \sigma \to \ln\gamma \quad \text{for ionic targets}\,,$$
$$\sigma \to \text{const} \quad \text{for atomic targets}, \tag{26}$$

whereas at nonrelativistic velocities the results obtained by the LOSS and LOSS-R codes coincide.

A rough approximation for $K_0$ in formulas (25) was made using the result of Bethe's paper [93] for estimating the energy transfer from ion to atom after collision event. Nevertheless, the results obtained by the LOSS-R code employing this simple approximation are in good agreement with both experimental data and more sophisticated but tedious calculations (see Section 3.1.3).

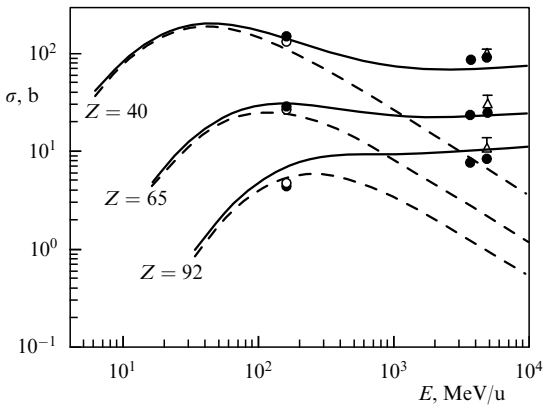


**Figure 5.** Proton-impact ionization cross sections of the K-shell electrons in neutral Zr, Tb, and U atoms as a function of proton energy. Experiment: triangles at collision energy 4.8 GeV [94]. Theory: white and dark circles — nonrelativistic and relativistic calculations, respectively, at 0.16, 3.672, and 4.88 GeV/u [95]; solid and dashed curves — relativistic (LOSS-R code) and nonrelativistic (LOSS) calculations, respectively (see Ref. [91]).

Experimental and theoretical data on K-shell ionization cross sections of neutral heavy atoms Zr ($Z = 40$), Tb ($Z = 65$), and U ($Z = 92$) by proton impact are shown in Fig. 5 at collision energies from tens of MeV/u to 10 GeV/u. As is seen, the nonrelativistic cross sections (the LOSS code) decrease with increasing collision energy, in accordance with the Born law (22), whereas the relativistic ones (the LOSS-R code) are slightly increasing for $E > 400$ MeV/u. At energy $E = 10$ GeV/u, the difference in cross-section values calculated by these codes reaches about one order of magnitude. In the energy range considered, experimental data [94], relativistic calculations [95], and LOSS-R results agree within 30%.

**3.1.2 The HERION code.** The problem of relativistic projectile ionization by neutral particles can be formulated in terms of the impact parameter ($b$) representation, when the electron-loss cross section is represented as a sum of dipole and nondipole terms:

$$\sigma(v) = \sigma_{\text{dip}}(v) + \sigma_{\text{nondip}}(v)\,. \tag{27}$$

The dipole cross section describes a contribution of ion–atom interactions at large impact parameters $b$, when the dipole interaction plays a key role, interaction between the projectile electrons and the target atom is weak, and transition of the active electron occurs with a small momentum transfer, so one can apply the perturbation theory. At small $b$ values, the interaction region turns out to be small but momentum transfer is large, and the impulse approximation may be used for cross-section calculations.

In the dipole approximation, the cross section $\sigma_{\text{dip}}(v)$ can be expressed via the projectile photoionization cross section $\sigma_{\text{ph}}(nl, \omega)$ and the so-called number $n(\omega)$ of equivalent photons (see Refs [96, 97]):

$$\sigma_{\text{dip}}(nl, v) = \int_{\omega_{\min}}^{\infty} n(\omega)\,\sigma(nl, \omega)\,\frac{\mathrm{d}\omega}{\omega}\,, \tag{28}$$

$$n(\omega) = \frac{2Z_{\text{eff}}^2}{\pi(\beta c)^2}\left[x K_0(x)\,K_1(x) - \frac{1}{2}(\beta x)^2\big(K_1^2(x) - K_0^2(x)\big)\right], \tag{29}$$

$$x = \frac{\omega b_{\min}}{\gamma\beta c}\,, \qquad b_{\min} = \frac{n}{(2I_{nl})^{1/2}}\,, \tag{30}$$

where $I_{nl}$ denotes the electron binding energy in the $nl$-shell of the projectile, $Z_{\text{eff}}$ is the effective target-atom charge, and $K_m(x)$ is the Macdonald function.

Employing the impulse approximation for the $\sigma_{\text{nondip}}(v)$ term yields [92]

$$\sigma_{\text{nondip}}(nl, v) = \frac{2\pi N_{nl}}{I_{nl}}\left(\frac{Z_{\text{eff}}\alpha}{\beta}\right)^2, \tag{31}$$

where $N_{nl}$ is the number of equivalent electrons in the $nl$-shell.

Equations (28)–(31) are implemented in the HERION code [92], where the relativistic Dirac–Fock wave functions are used for calculating the photoionization cross sections of heavy projectiles. The code is intended for the calculation of electron-loss cross sections at relativistic energies $E > 100$ MeV/u, and it does not account for the magnetic interactions between colliding particles and the $b$-dependence of the target effective charge.

The electron-loss cross sections calculated by the HERION and LOSS-R codes can differ by a factor of 2, which is mainly related to the employment of relativistic wave functions in the HERION code and nonrelativistic ones in the LOSS-R code. The HERION electron-loss cross sections mainly consist of a dipole part (60–70%) and, therefore, reproduce the shape of the total loss cross sections. The results obtained by the HERION code have turned out to be very useful for understanding the loss cross-section behavior at relativistic collision energies.

**3.1.3 Relativistic Born approximation: the RICODE program.** The general formulas for electron-loss cross sections of fast ion–atom collisions were obtained in paper [98] in the relativistic Born approximation, including magnetic interactions for ejection of the projectile electron from an arbitrary $nl$-shell. Based on these results, a RICODE computer program was created (see Refs [76, 99]). The code has the highest accuracy in calculating one-electron-loss cross sections of heavy ions by target ions and neutral atoms among those codes mentioned before (LOSS, LOSS-R, and HERION).

Formulas utilized in the RICODE program differ from expressions (17), (18) in the LOSS-R code by the presence of an additional term responsible for relativistic (magnetic) interaction between the projectile and the target atom, and have the form

$$\sigma_{\text{EL}}(v) = \frac{8\pi}{(\beta c)^2}\sum_{nl} N_{nl}\sum_{\lambda}\int_0^{\infty}\mathrm{d}\varepsilon \times \int_{K_0}^{\infty}\frac{\mathrm{d}K}{K^3}\left(F_{\text{T}}^2(Z_{\text{T}}, N_{\text{T}}, K)\,F_{nl}^2(\varepsilon, \lambda, K) + F_{\text{T}}^2(Z_{\text{T}}, N_{\text{T}}, K')\,\frac{\beta^2(1 - K_0^2/K^2)}{(1 - \beta^2 K_0^2/K^2)^2}\,G_{nl}^2(\varepsilon, \lambda, K)\right), \tag{32}$$

$$K_0 = \frac{I_{nl} + \varepsilon}{\beta c}\,, \qquad K' = \sqrt{K^2 - \beta^2 K_0^2}\,. \tag{33}$$

Here, $G_{nl}$ denotes the integral depending on the wave functions of the initial and final states, and on the derivative of the initial bound wave function $|nl\rangle$ (see paper [98] for details), and $F_{\text{T}}$ is the effective charge of the target atom defined in Section 3.1.

Equations (32), (33) were obtained in the relativistic Born approximation using the Coulomb gauge for the matrix

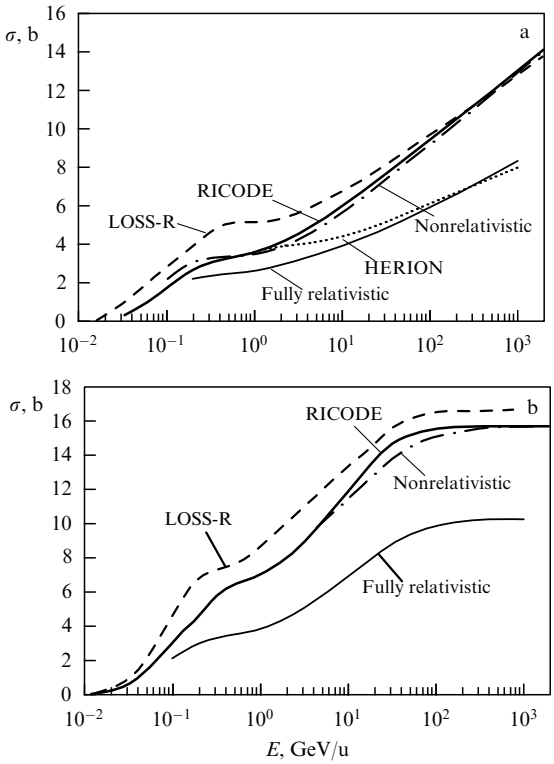


**Figure 6.** The Born cross sections of relativistic ionization of $U^{91+}(1s)$ ions by proton impact (a), and by collisions with H(1s) atoms (b) as a function of collision energy. The LOSS-R, RICODE, and HERION curves display the results obtained by the corresponding computer codes; dashed-dot curves — calculations with relativistic interaction and nonrelativistic wave functions, and thin solid curves — fully relativistic calculations [89, 90].

element (23), where the first and second terms in (32) correspond to the nonrelativistic and relativistic Born approximations, respectively. Relativistic effects for the form factor of the target atom were accounted for in the effective charge $F_T^2$ via momentum $K'$.

Similar to the LOSS and LOSS-R codes, the RICODE program utilizes the nonrelativistic radial wave functions for the bound and continuum states of an active electron. In the case of heavy many-electron projectiles, this is justified by the fact that the main contribution to the electron-loss cross section is made by the outer shells of the projectile, for which relativistic effects are small. On the contrary, in the case of few-electron heavy projectiles, the influence of relativistic effects on the wave functions is strong and leads to a few-fold reduction in the loss cross sections. This is illustrated in Fig. 6, where the calculated ionization cross sections of $U^{91+}(1s)$ projectiles in collisions with protons and H(1s) atoms are presented as a function of collision energy and compared with relativistic results (see paper [99]).

As is seen from Fig. 6, fully relativistic calculations for H-like uranium ions lead to a 2-fold reduction in the cross section compared to the results obtained by the RICODE program. It is also seen that the data obtained with the LOSS-R and RICODE programs are close to each other, and those with the HERION code are close to the fully relativistic calculations [89, 90], since the relativistic wave functions are used in the HERION code.

It should also be noted that all electron-loss cross sections calculated for collisions with protons increase logarithmically with collision energy, which is typical for collisions with charged particles, but cross sections tend to a constant value in collisions with neutral atoms in the limit of high relative velocities (see Fig. 6). The point is that in collisions with charged particles (protons, ions), the projectile-electron ionization occurs due to the long-range Coulomb interaction, and the cross section increases roughly as $\sigma \sim \ln\gamma$ [see formula (26)]. In collisions with neutral atoms, the active electron interacts with a screened atomic field which is Coulomb-like only at small distances and is exponentially small at large distances from the target (see paper [87] for details).

Another typical property of the electron-loss Born cross sections of heavy ions, following from results simulated by the LOSS, LOSS-R, and RICODE programs, is the possibility of scaling the cross sections $\sigma_{EL}$ on the target nuclear charge $Z_T$, i.e., for an ion with a fixed charge $q$ the $\sigma_{EL}$ quantity can be presented in the form $\sigma_{EL} \sim Z_T^{d(q)}$ in the whole energy range with about 20% accuracy. The $d(q)$ exponent depends on the electronic structure and the charge of the projectile and, as the ion charge increases, the $d(q)$ increases from approximately 1.2 to a maximum value of 1.8. This dependence is related to the screening effects in the target atoms: ionization of low-charged ions ($q \sim 1$) occurs at high impact parameters, when the target nucleus is strongly screened by atomic electrons, and for highly charged ions ($q \gg 1$) the electron ejection from the incident ion takes place at close distances to the target, where the screening effects mentioned are small (see paper [76] for details). The scaling feature of the Born electron-loss cross sections for heavy ions by atoms can be useful for cross-section estimations in collisions with an arbitrary target atom if the data for a fixed $Z_T$ value are known from experiment or sophisticated numerical calculations.

**3.1.4 Semiempirical formula for one-electron-loss cross sections.** Using the properties of the loss cross sections in the first Born approximation and numerical results obtained by the RICODE program, a semiempirical formula was devised in paper [76] for one-electron-loss cross sections in heavy ion–neutral atom collisions, covering a relativistic energy range:

$$\sigma\left[\frac{\text{cm}^2}{\text{atom}}\right] = 0.88\times10^{-16}(Z_T+1)^2\frac{u}{u^2+3.5} \times\left(\frac{\text{Ry}}{I_1}\right)^{1+0.01q}\left(4+\frac{1.31}{n_0}\ln(4u+1)\right), \quad (34)$$

$$u = \frac{v^2}{I_1/\text{Ry}} = \frac{(\beta c)^2}{I_1/\text{Ry}}, \quad (35)$$

where $v$ and $q$ denote the projectile velocity and charge, respectively, $c = 137$ is the speed of light, $u$ is the reduced projectile energy, $I_1$ is the projectile first ionization potential in Ry units, and $n_0$ stands for the principal quantum number of the projectile outer electron shell. The factor $(Z_T+1)^2$ in formula (34) is introduced instead of the usual $Z_T^2$ coefficient to get better agreement between the results obtained by using formula (34) and those by the RICODE program for light atomic targets like H, He, Li, Be, and B.

Cross section (34) reaches its maximum at $u \approx 2$:

$$\sigma_{\max}\left[\frac{\text{cm}^2}{\text{atom}}\right] \approx 10^{-16}(Z_T+1)^2\left(\frac{\text{Ry}}{I_1}\right)^{1+0.01q}, \qquad u_{\max}\approx 2\,. \quad (36)$$

As $v \to c$, cross section (34) tends to a constant quantity

$$\sigma\left[\frac{\mathrm{cm}^2}{\mathrm{atom}}\right] \approx 3\times 10^{-20}(Z_\mathrm{T}+1)^2\left(\frac{\mathrm{Ry}}{I_1}\right)^{0.01q}, \qquad u \approx c^2\,\frac{\mathrm{Ry}}{I_1}\,. \tag{37}$$

Semiempirical formula (34) for the electron-loss cross sections, together with formula (12) for electron-capture cross sections, can be applied for estimating the lifetimes of ion beams in accelerators and average charges of ions passing through gaseous targets (see Section 6).

### 3.2 Classical approximation

**3.2.1 Classical trajectory Monte Carlo (CTMC) approximation.** A large amount of theoretical data on electron-loss cross sections of heavy ions in collisions with atoms and molecules has been revealed in the classical approximation: by the CTMC method [68, 100] and the energy-deposition model [74]. The CTMC method was briefly discussed in Section 2.2. On the basis of the CTMC calculations of electron-loss cross sections for heavy projectiles, significant physical results have been obtained: a large contribution of multielectron loss to the total cross section at low and intermediate collision energies, a slower decreasing with velocity of the loss cross sections $\sigma_\mathrm{EL} \sim v^{-1}$ compared with the Born approximation ($\sigma_\mathrm{B} \sim v^{-2}$), a preferential one-electron loss at high collision energies, and some others.

**3.2.2 Energy-deposition method. The DEPOSIT code.** The classical energy-deposition model, suggested by N Bohr [101], is based on the assumption that if the kinetic energy $T(b)$ transferred to the projectile electrons in a collision with the target atom exceeds the first ionization potential $I_1$ of the projectile, $T(b) \geqslant I_1$, then the projectile can undergo one- or multi-electron ionization, where $b$ is the impact parameter.

The energy-deposition model was utilized in Ref. [102] to explain experimental data on many-electron ionization of the target *atoms* in collisions with *ions*. This model was further developed in paper [74] for ionization of *ions* by *atoms*, i.e., for computing electron-loss cross sections. It should be noticed that these two cases of ion–atom collisions are not identical: ionization of an *atom* by an ion occurs upon interaction of an atomic electron with a long-range Coulomb field of the projectile, whereas ionization of a *projectile* by an atom is due to active electron interaction with a field of the neutral target, which is close to the Coulomb one only at small interparticle distances and is exponentially small at large distances.

On the basis of the energy-deposition model, the DEPOSIT code was created [103] for calculating one- and many-electron-loss cross sections of projectiles in collisions with neutral atoms at low and intermediate energies. In the code, the atomic kinetic energy $T(b)$ transferred to the projectile electrons is calculated using the classical Bohr formula

$$T(b) = \sum_s \int \rho_s(r)\Delta E_\mathrm{se}(p)\,\mathrm{d}^3 r\,, \tag{38}$$

where $\rho_s(r)$ denotes the electron density of the projectile $s$-shell at a distance $r$ from its nucleus, $\Delta E_\mathrm{se}$ is the gain in kinetic energy of a single electron interacting with the target, $b$ is the impact parameter linking two nuclei, $p$ is the impact parameter linking the projectile electron and the target nucleus, and the sum over $s$ means summation over all projectile electrons. The vectors $\mathbf{r}$, $\mathbf{b}$, and $\mathbf{p}$ are related through a simple geometrical expression. The total electron density $\rho(r)$ is normalized to the total number $N$ of projectile electrons:

$$\int_0^\infty \sum_s \rho_s(r)\,\mathrm{d}r = \int_0^\infty \rho(r)\,\mathrm{d}r = \sum_s N_s = N\,. \tag{39}$$

In the DEPOSIT code, the shell electron density $\rho_s(r)$ is calculated using the Slater nodeless functions, and $\Delta E_\mathrm{se}$ via the derivative $\partial U(R)/\partial R$ of the field $U(R)$ created by the target atom at a distance $R$ from its nucleus. In the code, the analytical expression is used to describe the $U(R)$ field with five approximation parameters obtained by the Dirac–Hartree–Fock–Slater method for neutral atoms from H to U [104]:

$$U(R) = -\frac{Z_\mathrm{T}}{R}\sum_{i=1}^{3} A_i \exp\left(-\alpha_i R\right), \qquad \sum_{i=1}^{3} A_i = 1\,, \tag{40}$$

where $A_i$ and $\alpha_i$ are the approximation parameters.

As was mentioned, projectile ionization occurs under the condition

$$T(b) \geqslant I_1\,, \tag{41}$$

where $I_1$ is the first ionization potential of the projectile. Then, the total electron-loss cross section (summed over one- and multielectron-loss cross sections) has the form

$$\sigma_\mathrm{tot}(b) \equiv \sum_{m=1}^{N} \sigma_m = \pi b_\mathrm{max}^2\,. \tag{42}$$

Here, $\sigma_m$ denotes the $m$-electron-loss (ionization) cross section (Section 4.2), and the $b_\mathrm{max}$ value is found from the equation

$$T(b_\mathrm{max}) = I_1\,. \tag{43}$$

Therefore, the problem of finding the total electron-loss cross sections in the classical energy-deposition model is reduced to the calculation of the 3D integral (38) (cf., the CTMC method, Section 2.2). The calculation accuracy of this method is within a factor of 2, i.e., similar to that of the CTMC method. However, in the energy-deposition model there is no limitation on the total number of projectile electrons, unlike in the CTMC method, and, moreover, the heavier the colliding particles, the more accurate the results obtained in the model.

Electron-loss cross sections of $\mathrm{U}^{28+}$ ions colliding with $\mathrm{H}_2$, $\mathrm{N}_2$, Ar, Kr, and Xe targets are displayed in Fig. 7, where experimental data are compared with the CTMC and the DEPOSIT results (see Ref. [105]). As is seen from the figure, all experimental data agree with classical calculated results within a factor of 2, except for the $\mathrm{H}_2$ target, because the validity of the classical model for light targets and low collision energies is rather limited (see paper [103]).

The numerical results obtained by the DEPOSIT code allows one to examine the following high-energy behavior of the loss cross sections:

$$\sigma_\mathrm{EL} \sim E^{-a(Z_\mathrm{T})}\,, \qquad a(Z_\mathrm{T}) \approx \frac{0.8}{Z_\mathrm{T}^{0.3}}\,, \qquad v^2 \gg I_1\,, \tag{44}$$

where $a(\mathrm{H}) = 0.80$, $a(\mathrm{Ne}) = 0.40$, $a(\mathrm{Ar}) = 0.34$, $a(\mathrm{Xe}) = 0.24$, and $a(\mathrm{U}) = 0.21$. As is seen, the heavier the target atom, the

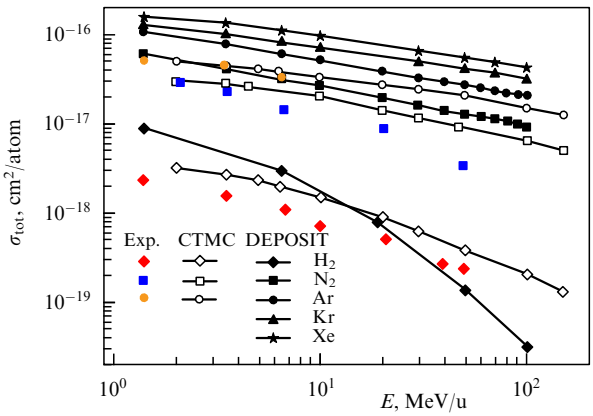


**Figure 7.** (Color online.) The total electron-loss cross sections of $U^{28+}$ ions colliding with $H_2$, $N_2$, Ar, Kr, and Xe targets as a function of ion energy. Experiment: red symbols — $H_2$ target, blue symbols — $N_2$ target, orange symbols — Ar target (taken from Refs [44,68, 100, 106]). Theory: curves with white symbols — CTMC result, curves with the black symbols — energy-deposition model, DEPOSIT code (see Ref. [105]).

slower the cross section decreases that is related to the different contributions of multielectron processes to the total cross section (see Section 4.2). From formula (44) it follows that the classical electron-loss cross section $\sigma_{cl}$ decreases much more slowly with energy than the Born cross section $\sigma_B$:

$$\sigma_{cl} \sim E^{-a}\,, \qquad a < 1\,, \qquad \sigma_B \sim \frac{\ln E}{E}\,, \qquad v^2 \gg I_1\,. \tag{45}$$

The validity conditions for the classical energy-deposition model with the target potential (40) have been obtained in Ref. [103] in the form

$$R_A \left(\sum_s N_s r_s^2\right)^{-1/2} \left(\frac{2I_1}{Z_T}\right)^{1/2} < v < \frac{2R_A}{R_{ion}} \left(\frac{2I_1}{Z_T}\right)^{1/2}, \tag{46}$$

where $R_A$ and $R_{ion}$ denote the target and projectile sizes, respectively, and $r_s$ is the size of the $s$-shell of the projectile. The lower limit on velocity in formula (46) follows from condition (41) for the minimum transferred kinetic energy exceeding the first ionization potential of the projectile. The upper limit is resulted from the classical condition that the collision time is small, and the gain $\Delta u_s$ of the electron orbital velocity by collision is smaller than its absolute value: $\Delta u_s \ll u_s$.

Numerical calculations of the total electron-loss cross sections show that the classical approach in the deposit-energy representation gives reasonable results for the ion velocities (in atomic units) ranging $0.1 < v < 10$ a.u., 1 a.u. $\approx 2.2 \times 10^8$ cm s$^{-1}$.

## 4. Multielectron processes in ion–atom collisions

If heavy projectiles are involved in electron-loss and capture processes, multielectron mechanisms of charge transfer play a very important role and lead to a significant contribution to the total cross sections, depending on the relative velocity and atomic structure of colliding particles. This is demonstrated in Table 1, where experimental data on one-electron and total charge-changing cross sections are given for collisions of uranium ions with Ar atoms at $E = 3.5$ MeV/u [45]. As is seen, the contribution of multielectron loss processes

**Table 1.** Experimental electron-loss and electron-capture cross sections (in $10^{-18}$ cm$^2$) for collisions of $U^{q+}$ ions, $q = 28-51$, with Ar atoms at $E = 3.5$ MeV/u [45].

| Ion charge $q$ | $\sigma_{EL}^{(1)}$ | $\sigma_{EL}^{(tot)}$ | $\sigma_{EC}^{(1)}$ | $\sigma_{EC}^{(tot)}$ |
|---|---|---|---|---|
| 28 | 13.4 | 40.6 | 12.6 | 12.6 |
| 31 | 12.5 | 34.7 | 19.7 | 20.8 |
| 33 | 8.7 | 26.3 | 25.0 | 27.0 |
| 39 | 8.0 | 19.7 | 52.3 | 60.7 |
| 42 | 6.7 | 13.8 | 61.6 | 79.7 |
| 51 | — | — | 82.5 | 130 |

$\sigma_{EL}^{(1)}$ and $\sigma_{EL}^{(tot)}$ are the one-electron and total loss cross sections, and $\sigma_{EC}^{(1)}$ and $\sigma_{EC}^{(tot)}$ are the one-electron and total capture cross sections, respectively.

decreases from 70 to 50% upon increasing the projectile charge, and that of multielectron capture processes increases from 0 to 40%.

### 4.1 Multielectron capture

Experimental data on multielectron capture in slow ($E = 0.01$ eV/u – 10 keV/u) ion–atom collisions

$$X^{q+} + A \to X^{(q-k)+} + A^{k+}\,, \qquad k \geqslant 1\,,$$

can be found in Refs [107–115].

For heavy low-charged ions, the corresponding cross sections in collisions with noble gases and molecules were reported in Refs [108, 109] for the following reactions:

$$\begin{aligned} &X^{q+} + A \to X^{(q-k)+} + A^{k+}\,, \qquad k \geqslant 1\,, \qquad 2 \leqslant q \leqslant 8\,, \\ &X = \mathrm{Ne, Ar, Kr, Xe}\,, \\ &A = \mathrm{He, Ne, Ar, Kr, Xe, H_2, N_2, O_2, CH_4, CO_2}\,. \end{aligned} \tag{47}$$

These data demonstrate a semiconstant behavior of the capture cross sections at low energies, while experimental cross sections for capture of $k$-electrons, $k \leqslant 4$, were approximated well by the simple formula [109]

$$\sigma_{q,q-k}\,[\mathrm{cm}^2] = 10^{-12} C(k) q^{A(k)} \left(\frac{I_T}{\mathrm{eV}}\right)^{-B(k)}, \quad q \leqslant 8\,, \; v \ll 1\,\text{a.u.}, \tag{48}$$

where $I_T$ is the ionization potential of a target atom, and $C$, $A$, and $B$ are the approximation parameters given in Table 2.

**Table 2.** Approximation parameters for experimental $k$-fold electron capture cross sections (48) at small relative velocities $v \ll 1$ a.u. $\approx 2.2 \times 10^8$ cm s$^{-1}$ (taken from Ref. [109]).

| $k$ | $C(k)$ | $A(k)$ | $B(k)$ |
|---|---|---|---|
| 1 | $1.43 \pm 0.76$ | $1.17 \pm 0.09$ | $2.76 \pm 0.19$ |
| 2 | $1.08 \pm 0.95$ | $0.71 \pm 0.14$ | $2.80 \pm 0.32$ |
| 3 | $(5.50 \pm 5.8) \times 10^{-2}$ | $2.10 \pm 0.24$ | $2.89 \pm 0.39$ |
| 4 | $(3.57 \pm 8.9) \times 10^{-4}$ | $4.20 \pm 0.79$ | $3.03 \pm 0.86$ |

Experimental data on multielectron capture of $Xe^{q+}$ ions, $15 \leqslant q \leqslant 43$, colliding with He, Ar, and Xe atoms at slow collision velocities $v = 0.1-0.2$ a.u. are presented in paper [113], and in paper [114] these data were approximated by falling back on a semiempirical formula. Experimental multielectron capture cross sections for slow ions colliding with atoms and molecules are given in Refs [116–118]. It is worth noting the results of experimental [119–121] and theoretical [119, 122] studies of one- and multielectron capture cross sections involving fullerenes (hexagonal carbon rings); these

data are of a particular interest for electron capture in ion collisions with complex targets.

Experimental three-electron capture cross sections of highly charged ions (from $Ne^{6+}$ up to $U^{48+}$) colliding with Ar atoms at energy $E = 1.4$ MeV/u obtained by the coincidence technique are presented in paper [117]; these data are quite well described by the CTMC method. At higher energies $E = 1-10$ MeV/u, experimental data are mainly obtained for heavy Xe, Pb, and U ions colliding with gaseous targets (see Refs [44, 45, 82, 100]).

Theoretical investigations into multielectron capture processes are rather limited and refer mainly to low and intermediate collision energies. First and foremost, one has to mention here the classical Bohr–Lindhard model [123] developed later in papers [124, 125]; this model is primarily used for capture processes involving few-electron projectiles. Numerical calculations of the multielectron capture cross sections have been generally performed for two-electron capture using the close-coupling method [126–128], the quasimolecular model [129], and the independent-particle model (IPM) [130]. As for theoretical models for multielectron capture ($k > 2$) by heavy ions from atoms, one has to admit that at present they are somewhat incompletely developed (see Refs [122, 125, 131]).

### 4.2 Multielectron loss

The probability of multielectron loss of heavy ions in the reactions

$$X^{q+} + A \to X^{(q+m)+} + \sum A + me^- , \qquad m \geqslant 1 ,$$

can be high, and the contribution of the corresponding cross section to the total one can reach more than 50%. This property is demonstrated in Table 3, where experimental data for one- and multielectron loss cross sections are presented. As is seen, the contribution of multielectron loss processes increases with the target atomic number and decreases with the projectile charge $q$.

**Table 3.** Experimental $m$-fold electron-loss cross sections $\sigma_m$ ($m = 1, 2, 3$) and the total electron-loss cross sections $\sigma_{tot}$ (in $10^{-18}$ cm$^2$) in collisions of $Xe^{18+}$ (ionization potential $I_1 = 573$ eV) and $Ar^{8+}$ ($I_1 = 420$ eV) ions with noble gas atoms.

| Process | Energy, MeV/u | $\sigma_1$ | $\sigma_2$ | $\sigma_3$ | $\sigma_{tot}$ | References |
|---|---|---|---|---|---|---|
| $Xe^{18+} + He$ | 6 | 3.0 | 1.7 | 0.2 | 4.9 | [132] |
| $Xe^{18+} + Ne$ | 6 | 16 | 7.8 | 3.8 | 36 | [132] |
| $Xe^{18+} + Ar$ | 6 | 24 | 11 | 5.6 | 56 | [132] |
| $Xe^{18+} + Kr$ | 6 | 27 | 13 | 7.2 | 75 | [132] |
| $Xe^{18+} + Xe$ | 6 | 34 | 16 | 9.0 | 95 | [132] |
| $Ar^{8+} + Xe$ | 19 | 23 | 10 | 5.5 | 44 | [133] |

The multielectron ionization theory leads to the result that the cross section of $m$-fold electron loss can be expressed in the impact-parameter representation in the form

$$\sigma_m(b) = 2\pi \int_0^\infty P_m(b) b \, \mathrm{d}b , \tag{49}$$

where $P_m(b)$ denotes the ionization probability of $m$ electrons of the projectile as a function of the impact parameter $b$. The total loss cross section, summed over all $m$, is given by

$$\sigma_{tot}(v) = \sum_{m=1}^{N} \sigma_m(v) , \tag{50}$$

where $N$ is the total number of the projectile electrons. Usually, it is enough to include terms up to $N = 18$ whereat sum (50) converges very fast.

In the CTMC method, the $P_m(b)$ quantities are found numerically by solving a large number of differential equations (see Section 2.2). In the DEPOSIT code (Section 3.2.2), on the contrary, an analytical expression for $P_m(b)$ finds application in the statistical Russek–Meli model [134]:

$$P_m(b) = \binom{N}{m} S_m\left(\frac{E_K}{I_1}\right) \left[\sum_{i=1}^{N} \binom{N}{i} S_i\left(\frac{E_K}{I_1}\right)\right]^{-1} , \tag{51}$$

$$\sum_{m=1}^{N} P_m(b) = 1 ,$$

$$E_K = T(b) - \sum_{i=1}^{m} I_i , \qquad S(x) = \frac{2^{[(m-1)/2]} \pi^{[m/2]} x^{(3m-2)/2}}{(3m-2)!!} , \tag{52}$$

where $\binom{N}{m}$ denotes the binomial coefficient, $T(b)$ is the energy transferred to the projectile by the target, $I_i$ is the $i$th ionization potential of the projectile, $E_K$ is the kinetic energy of an ejected electron in $m$-fold ionization, and $[a]$ denotes the integer part of $a$. The electron binding energies of heavy atoms and ions are presented in tables [77–80]. As seen from formula (51), the Russek–Meli probability $P_m(b)$ strongly depends on the donated energy $T(b)$.

The dependences of $T(b)$ and $P_m(b)$ functions on the impact parameter $b$, which were calculated by the DEPOSIT code for collisions of $Xe^{18+}$ ions with Xe atoms at energy $E = 6$ MeV/u ($v = 15.5$ a.u.) are depicted in Fig. 8 (see paper [103]). The contribution from different electron shells of $Xe^{18+}$ ions to the total energy transfer $T(b)$ is shown in Fig. 8a, and Fig. 8b displays the ionization probability $P_m(b)$ for the same case as a function of $b$. At each value of $b$, the sum of $P_m(b)$ over all $m$ electrons is equal to unity

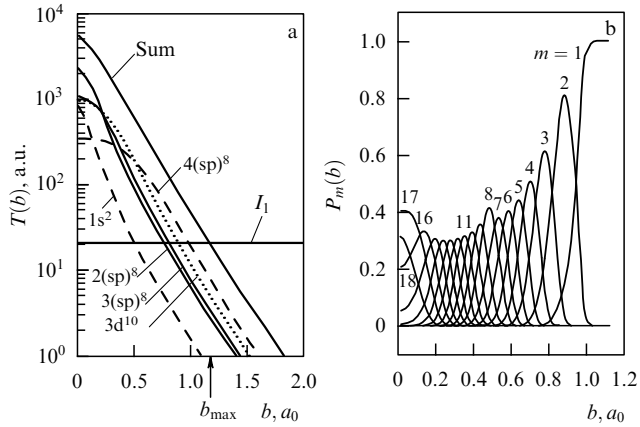


**Figure 8.** (a) Energy $T(b)$ transferred to $Xe^{18+}$ ions by collisions with Xe atoms at $E = 6$ MeV/u ($v = 15.5$ a.u.) as a function of impact parameter $b$: the result of the DEPOSIT code [103]. A contribution from different electron shells of $Xe^{18+}$ to the total (sum) donated energy is shown. Horizontal line $I_1 = 21$ a.u. (572.5 eV), corresponding to the first ionization potential of an $Xe^{18+}$ ion, indicates the minimum transferred energy required for ion ionization, and $b_{max}$ shows the impact parameter corresponding to the total electron-loss cross section. The notation of the shell, e.g., 2(sp)$^8$, means the electron configuration $2s^2 2p^6$. (b) The result of the DEPOSIT code for the multielectron ionization probability $P_m(b)$ as a function of $b$ was obtained using formula (51) with the transferred energy $T(b)$ shown in Fig. 8a [103]; $a_0$ is the Bohr radius.

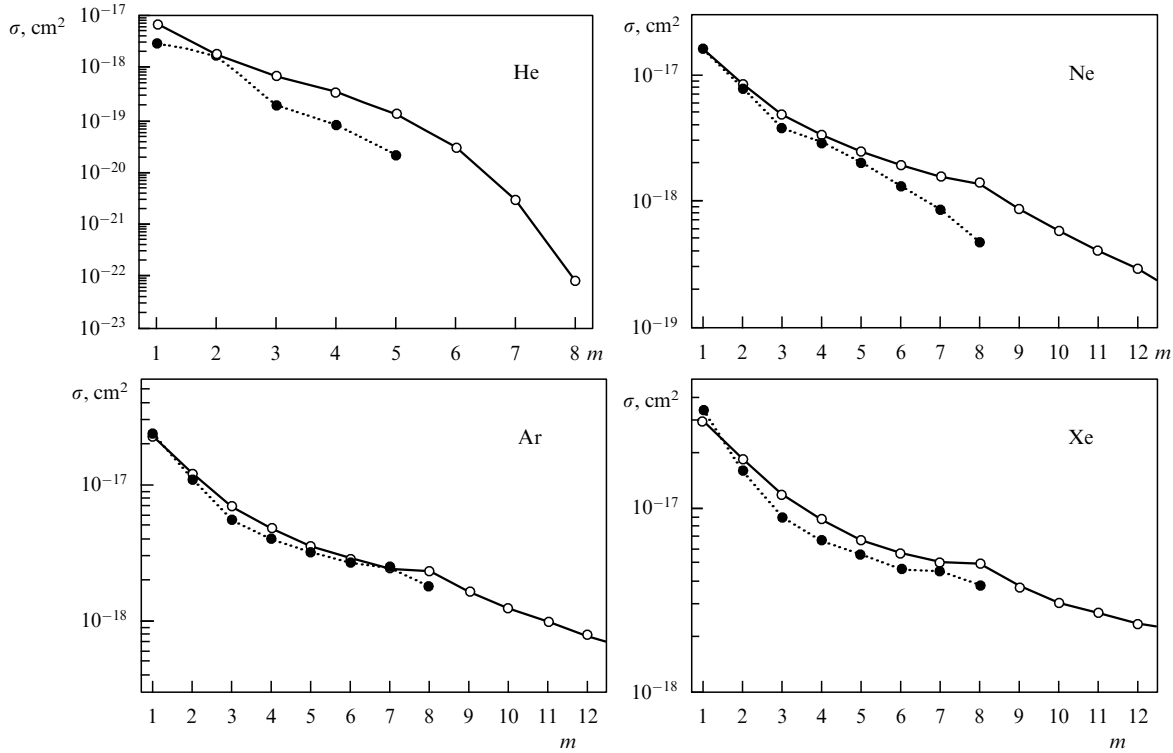


**Figure 9.** The $m$-fold electron loss cross sections for collisions of $Xe^{18+}$ ions with He, Ne, Ar, and Xe atoms at the ion energy $E = 6$ MeV/u as a function of $m$. Experiment: dotted curves with black circles [132]. Theory: solid curves with white circles simulated by the DEPOSIT code [132].

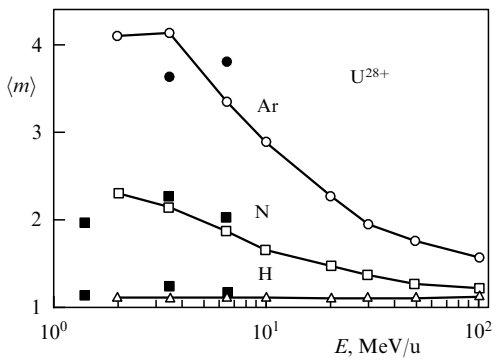


**Figure 10.** Average number $\langle m \rangle$ (53) of projectile electrons ejected from $U^{28+}$ ions upon collisions with H, N, and Ar atoms as a function of the projectile energy. Experiment: black symbols at $E = 1.4$ MeV/u [44], at 3.5 and 6.5 MeV/u [45, 68]. Theory: solid curves with white symbols — the CTMC calculated results [100].

according to formula (51). The $m$-electron loss cross sections of $Xe^{18+}$ ions colliding with He, Ne, Ar, and Xe atoms at $E = 6$ MeV/u, calculated by the DEPOSIT code [105], are shown in Fig. 9 in comparison with available experimental data [132].

Experimental investigations of multielectron-loss cross sections of heavy ions and theoretical calculations via the CTMC code [68, 100] showed that, upon increasing the collision energy, the contribution of multielectron losses decreases and one-electron loss processes begin to play a key role. This fundamental result is illustrated in Fig. 10, where the average number $\langle m \rangle$ of ejected electrons, namely

$$\langle m \rangle = \frac{\sum_m m\sigma_m}{\sum_m \sigma_m}\,, \tag{53}$$

is displayed for one collision event with a $U^{28+}$ ion impinging on H, N, and Ar atoms as a function of the projectile energies $E = 1-100$ MeV/u. As is seen, in a single collision of the $U^{28+}$ ion with the Ar atom, four electrons on the average, $\langle m \rangle = 4$ (!), are ejected for low energies $E < 10$ MeV/u, and the only one, $\langle m \rangle = 1$, at high energies.

Systematic investigations into the scaling laws for one- and multielectron-loss cross sections in ion–atom collisions have been performed in Refs [135, 136] over a wide range of collision energies. There, the authors have systematized the properties of experimental electron-loss cross sections and their dependences on the collision energy and atomic parameters, such as the projectile ion charge and the target atomic number, and quantum numbers of the active electrons. The scaling laws obtained describe experimental data within a factor of 2.

We note that, at present, there is no unique theoretical approach to describing electron-loss cross sections over a wide energy range, so in applications one has to lean upon some semiempirical methods to obtain the so-called recommended cross sections, which are found by applying different theoretical methods at low- and high-collision energies, and their further matching at intermediate energies (see Section 4.3).

### 4.3 Recommended electron-capture and electron-loss cross sections

The electron capture processes and theoretical methods of their calculation were considered in Section 2 over a wide collision energy range. It was shown that one-electron-capture cross sections involving heavy ions with energy $E > 10$ keV/u can be calculated using the normalized Brinkman–Kramers approximation implemented in the CAPTURE code. At lower energies, $E < 10$ keV/u, the best

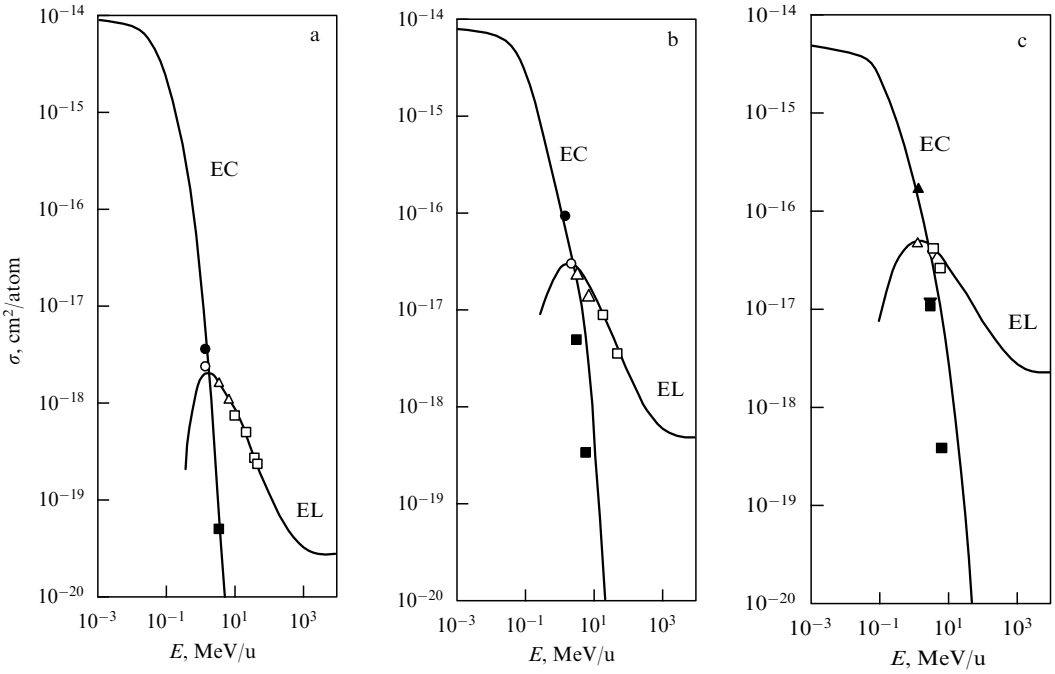


**Figure 11.** Recommended electron-capture (EC) and electron-loss (EL) cross sections of $U^{28+}$ ions colliding with $H_2$ (a), $N_2$ (b), and Ar (c) targets as a function of ion energy, solid curves [76]. Experiment, figures a, b: EC cross sections — black circles [82], black squares [100]; EL cross sections — white circles [82], white triangles [100], white squares [138]. Experiment, figure c: EC cross sections — black triangle up [44], black square [100], black triangle down [45]; EL cross sections — white triangle up [44], white square [68], white triangle down [45].

results are found with the aid of a close-coupling method and adiabatic-transition theory (see Section 7).

In the case of electron-loss processes, calculations of their associated cross sections are performed using different approximations as well: at low and intermediate energies — the classical approximation, which describes the multielectron and total cross sections, and at higher energies, including the relativistic range — the relativistic one-electron Born approximation.

Since, at present, there is no unique theory describing the electron-loss cross sections in the whole energy range considered, $E = 1$ keV/u–10 GeV/u, one has, in practice, to match the classical and quantum-mechanical cross sections for obtaining the so-called recommended cross-section data. For this purpose, a simple formula for the recommended electron-loss cross sections was made up, which is similar to that defining the reduced mass of two particles:

$$\frac{1}{\sigma_{\rm rec}} = \frac{1}{\sigma_{\rm DEPOSIT}} + \frac{1}{\sigma_{\rm RICODE}}\,, \tag{54}$$

where $\sigma_{\rm rec}$ denotes the recommended cross section, and $\sigma_{\rm DEPOSIT}$ and $\sigma_{\rm RICODE}$ are the cross sections calculated using the classical approximation via the DEPOSIT code and the quantum-mechanical one via the RICODE program, respectively. This method allows one to describe effectively the electron-loss cross sections over a wide energy range, including intermediate energies, where calculations are very complicated. A formula similar to Eqn (54) was used in work [137] for matching electron-impact ionization cross sections of positive ions at low and high electron energies.

The recommended charge-changing cross sections [combined results of the DEPOSIT and RICODE programs, and formula (54)] for $U^{28+}$ ions colliding with H, N, and Ar atoms at collision energies $E = 1$ keV/u–10 GeV/u are presented in Fig. 11 [76] in comparison with available experimental data. Similar data for other uranium ions are given in paper [85], where the recommended loss cross sections were approximated by 7th-order polynomials. The data presented in an analytical form are required for many applications, e.g., for estimating the lifetimes of the ion beams in accelerators, determining the mean ion charges in penetrating ions through gaseous targets, and so forth (see also Section 6).

## 5. Target density effects

The target density (or gas–solid) effect was discovered experimentally and described by Lassen [139, 140] in measuring the charge-state fractions of a uranium ion beam passing through carbon foils and gas targets, and later [141] in experiments on comparing the stopping power of ion beams in gaseous and solid media. Initially, the term 'target density effect' was introduced to indicate the increase in the equilibrium mean charge of ion beams penetrating through solid targets, as opposed to gaseous ones. The first theoretical models for interpretation of the effect considered on the ion charge-state fractions and stopping power were constructed in Refs [123, 142]. Later on, with the development of the accelerator technique, experimental and theoretical investigations of the density effect have been continued in Refs [27, 143–146]. At the present time, the term 'target density effects' is regarded in a wider sense, meaning also their influence on the effective cross sections of atomic processes, on the stopping power of ion beams in a dense media, on equilibrium charge states of ion beams passing through a plasma or foil targets, and so on.

In the previous sections of this review, charge-changing processes (electron capture and electron loss) occurring in binary ion–atom collisions were considered, namely at low target densities. However, the collision frequency increases

with increasing target density, and the time intervals between two neighboring collision events become shorter than the lifetime of the projectile excited states, so that a considerable part of the ions, already in excited states, undergo further collisions with the medium particles. Excited ions cannot be stabilized by transitions into lower quantum states through the radiative or other mechanisms because they are ionized at ensuing collisions with the target particles.

As a result of target density effects, the electron-capture cross sections decrease with increasing target density, while the electron-loss ones increase. These properties have been revealed experimentally in Refs [145, 147, 148]. The combined influence of both ion–atom collision peculiarities, as is seen below, leads to an increase in the equilibrium ion charge in a more dense medium.

### 5.1 Influence of target density effects on electron-capture cross sections

For simplicity, let us consider the influence of target density effects on electron-capture cross sections for a charge-exchange reaction when the resulting ion is created in a state with a specific principal quantum number $n$:

$$\mathrm{X}^{q+} + \mathrm{A} \to \mathrm{X}^{(q-1)+*}(n) + \mathrm{A}^{+}\,, \tag{55}$$

where the asterisk stands for an excited state.

In a low-density medium (a rarefied gas), the $\mathrm{X}^{(q-1)+}(n)$ ions are created in all possible quantum states $n$: from the ground $n_0$ up to highly excited states $n \gg 1$; then, the total electron-capture cross section has the form of the sum taken over all $n$-states:

$$\sigma_{\mathrm{tot}}(v) = \sum_{n=n_0}^{\infty} \sigma_n(v)\,. \tag{56}$$

As the target density increases, a certain number of ions emerge in the state with the maximum principal quantum number $n_{\mathrm{cut}}$, so that the $\mathrm{X}^{(q-1)+}(n)$ ions with $n > n_{\mathrm{cut}}$ are ionized by the medium particles in subsequent collisions, and $\mathrm{X}^{(q-1)+}(n)$ ions with $n \leqslant n_{\mathrm{cut}}$ are stabilized via radiative transitions to the ground state. Then, the total electron-capture cross section with account for the density effects, $\sigma_{\mathrm{DE}}$, is defined by sum (56) over $n$ but with the finite upper limit:

$$\sigma_{\mathrm{tot}}^{\mathrm{DE}}(v) = \sum_{n=n_0}^{n_{\mathrm{cut}}} \sigma_n(v)\,. \tag{57}$$

Therefore, the number of 'surviving' $\mathrm{X}^{(q-1)+}(n)$ ions decreases with the target density increasing, resulting in a capture cross-section reduction.

The cut-off parameter $n_{\mathrm{cut}}$ can be estimated from the equation of balance between ionization rate and the probability of radiation decay of the excited state:

$$\rho_{\mathrm{T}} v \sigma_{\mathrm{EL}}(n_{\mathrm{cut}}) = A(n_{\mathrm{cut}})\,, \tag{58}$$

where $\rho_{\mathrm{T}}$ denotes the target density, $\sigma_{\mathrm{EL}}$ is the electron-loss (ionization) cross section of the $\mathrm{X}^{(q-1)+}(n)$ ion by the target atoms, and $A(n)$ is the total radiation decay probability of the excited $n$-state.

Using the classical Thomson formula for ionization cross section $\sigma_{\mathrm{EL}}$ and the classical Kramers formula for the total decay probability $A(n)$, one can estimate the dependences of the $n_{\mathrm{cut}}$ quantity on the atomic parameters (see Ref. [65]):

$$\begin{aligned} &\sigma_{\mathrm{EL}} \sim \frac{Z_{\mathrm{T}}^2 n^2}{q^2 v^2}\,, \qquad A(n) \sim \frac{q^4}{n^5}\,, \\ &n_{\mathrm{cut}} \approx q\left(\frac{10^{18}}{Z_{\mathrm{T}}^2\,\rho_{\mathrm{T}}\,[\mathrm{cm}^{-3}]}\right)^{1/7}\left(\frac{v^2}{10q^2}\right)^{1/14} \\ &\qquad \approx q\left(\frac{10^{18}}{Z_{\mathrm{T}}^2\,\rho_{\mathrm{T}}\,[\mathrm{cm}^{-3}]}\right)^{1/7}\left(\frac{E\,[\mathrm{keV/u}]}{250q^2}\right)^{1/14}, \end{aligned} \tag{59}$$

where $E$ is the projectile energy. As is seen, the target density effects are large (i.e., $n_{\mathrm{cut}}$ is small) when the density $\rho_{\mathrm{T}}$ and the target nuclear charge $Z_{\mathrm{T}}$ are large, and also when the projectile charge $q$ and energy $E$ are small. Although formula (59) is approximate, it exhibits the main dependences of the cut-off parameter $n_{\mathrm{cut}}$ on the target density and other atomic parameters. In practice, a more strict condition for the 'dense' target may be set for a more accurate estimation of the $n_{\mathrm{cut}}$ quantity:

$$\frac{\rho_{\mathrm{T}} v \sigma_{\mathrm{EL}}(n_{\mathrm{cut}})}{A(n_{\mathrm{cut}})} \gg d\,, \tag{60}$$

where $d$ is a constant, $d > 1$. For example, if $d = 10$, then 90% of ions with the principal quantum number $n_{\mathrm{cut}}$ are ionized, and 10% are radiatively stabilized into the ground state. The cut-off parameter $n_{\mathrm{cut}}$ has a weak dependence on $d$, $n_{\mathrm{cut}} \sim d^{1/7}$, as follows from formula (59).

The ionization rate $\rho v \sigma$ and the total radiative decay probability into the ground 1s-state of $\mathrm{O}^{6+}(n)$ ions created in electron capture reaction $\mathrm{O}^{7+} + \mathrm{He} \to \mathrm{O}^{6+}(n) + \mathrm{He}^{+}$ at energy $E = 3.2$ MeV/u are plotted in Fig. 12 as a function of the principal quantum number $n$ at helium densities $\rho = 10^{13}$ and $10^{19}$ cm$^{-3}$. As seen from the figure, the maximum principal quantum number $n_{\mathrm{cut}}$ of the resulting $\mathrm{O}^{6+}$ ions is $n_{\mathrm{cut}} \approx 30$ at $\rho = 10^{13}$ cm$^{-3}$, whereas the $n_{\mathrm{cut}}$ value at $\rho = 10^{19}$ cm$^{-3}$ is much lower: $n_{\mathrm{cut}} \approx 3$. The increasing of the target density leads to a reduction of the capture cross section to about one order of magnitude — from $5.5 \times 10^{-16}$ to $8.0 \times 10^{-17}$ cm$^2$ (see Ref. [149] for details).

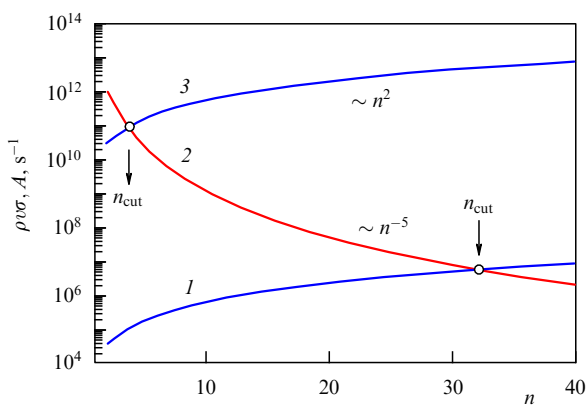


**Figure 12.** (Color online.) Electron-loss (ionization) rate $\rho v \sigma$ (curves *1*, *3*) and the total radiative decay probability $A(n)$ (curve *2*) for the $n$-states of the $\mathrm{O}^{6+}(n)$ ions created in the electron-capture reaction $\mathrm{O}^{7+} + \mathrm{He} \to \mathrm{O}^{6+}(n) + \mathrm{He}^{+}$ at $E = 3.2$ MeV/u as a function of $n$: curve *1* for the helium density $\rho = 10^{13}$ cm$^{-3}$, and curve *3* for $\rho = 10^{19}$ cm$^{-3}$ [149]. The crossing points show maximal principal quantum numbers $n_{\mathrm{cut}}$ with which $\mathrm{O}^{6+}$ ions survive in collisions with helium atoms at two different He densities [see formula (57)].

Numerical calculations of electron-capture cross sections showed that the reduction of the cross sections due to the density effects can be very large (more than 10 times) depending on the cut-off parameter $n_{\rm cut}$ which, in turn, is a function of the ion energy and electronic structure of colliding particles. In other words, the absolute target density can be small but the target density effects are large.

### 5.2 Influence of target density effects on electron-loss cross sections

Similar formulas as derived in previous Section 5.1 for electron-capture cross sections with due regard for target density effects can be obtained for electron-loss cross sections (projectile ionization):

$$\mathrm{X}^{q+}(n_0) + \mathrm{A} \to \mathrm{X}^{(q+1)+} + \mathrm{A} + \mathrm{e}^- , \qquad (61)$$

where $n_0$ denotes the principal quantum number of the projectile ground state, and A is the target atom.

As the target density increases, electron-loss processes will include, besides ionization from the ground $n_0$-state, ionization from excited $n$-states of the projectile ions created due to collisions with the target atoms, so that the total ionization cross section $\sigma_{\rm ion}^{\rm DE}(v)$ of the projectile ion $\mathrm{X}^{q+}(n_0)$ with the density effects included can be written out as

$$\sigma_{\rm ion}^{\rm DE}(v) = \sigma_{\rm ion}(n_0) + \sum_{n>n_0} \sigma_{\rm ion}(n)\, B(n) , \qquad (62)$$

$$B(n) = \frac{\rho_{\rm T} v \sigma_{\rm ex}(n_0 - n)}{A(n) + \rho_{\rm T} v \sigma_{\rm de\text{-}ex}(n - n_0) + \rho_{\rm T} v \sigma_{\rm ion}(n)} , \qquad (63)$$

where $B(n)$ denotes the branching ratio of the excited level $n$, $\sigma_{\rm ion}(n_0, n)$ are ionization cross sections from the $n_0$ and $n$ levels without regard for the density effects, $\sigma_{\rm ex}(n_0 - n)$ and $\sigma_{\rm de\text{-}ex}(n - n_0)$ denote, respectively, excitation and deexcitation cross sections of the projectile by the target atoms, and $A(n)$ is the total radiative decay probability of the $n$-state. The $\sigma_{\rm ex}$ and $\sigma_{\rm de\text{-}ex}$ quantities for the $n_0 - n_1$ transition are related by the Klein–Rosseland formula [150]

$$g_0 \left( \frac{v^2}{2} + \Delta E \right) \sigma_{\rm de\text{-}ex}\left( \sqrt{v^2 + \Delta E} \right) = g_1 \frac{v^2}{2} \sigma_{\rm ex}(v) , \qquad (64)$$

where $\Delta E$ denotes the excitation energy for the $n_0 - n_1$ transition, and $g_{0,1}$ are the statistical weights of the initial and final states: $g_0 = 2n_0^2$, and $g_1 = 2n_1^2$.

Taking into consideration that $v^2 \gg \Delta E$ for fast ions, and that

$$\sigma_{\rm ion}(n) \sim n^2 , \quad \sigma_{\rm ex}(n_0 - n) \sim n^{-3} , \quad \sigma_{\rm de\text{-}ex}(n_0 - n) \sim n^{-1} , \qquad (65)$$

the $B(n)$ ratio can be written out in the form

$$B(n) = \frac{\rho_{\rm T} v \sigma_{\rm ion}(n)}{A(n) + \rho_{\rm T} v \sigma_{\rm ion}(n)} . \qquad (66)$$

Using estimates (65) and assuming that the main contribution to sum (62) is made by excitation to and ionization from the resonance level $n_{\rm r}$ (i.e., electric-dipole-allowed transition to the ground state $n_0$), one finally arrives at the following expression for the electron-loss (ionization) cross section, including the density effects:

$$\sigma_{\rm ion}^{\rm DE}(v) = \sigma_{\rm ion}(n_0) + \sigma_{\rm ex}(n_0 - n_{\rm r})\, B(n_{\rm r}) , \qquad (67)$$

where $\sigma_{\rm ex}(n_0 - n_{\rm r})$ denotes the excitation cross section for the resonant transition $n_0 - n_{\rm r}$, and $n_{\rm r}$ is the principal quantum number of the resonance level, and the $B(n_{\rm r})$ coefficient is defined in relation (66).

Equation (67) shows the main dependences of the loss cross section on the target density and other parameters, and can easily be generalized to the case of ionization from levels with the orbital quantum numbers $nl$ [149].

For low-density targets (a rarefied gas), the branching ratio $B \to 0$ and the electron-loss cross section is given by the 'usual' formula for binary collisions:

$$\sigma_{\rm ion}^{\rm DE}(v) \approx \sigma_{\rm ion}(n_0) , \qquad \rho_{\rm T} \to 0 , \qquad B \to 0 . \qquad (68)$$

For very dense targets (solid state), the coefficient $B \to 1$ and the loss cross section is defined by the sum of ionization cross section from the ground state and excitation cross section from the ground state to the resonance one:

$$\sigma_{\rm ion}^{\rm DE}(v) \approx \sigma_{\rm ion}(n_0) + \sigma_{\rm ex}(n_0 - n_{\rm r}) , \qquad \rho_{\rm T} \to \infty , \qquad B \to 1 . \qquad (69)$$

Since

$$\sigma_{\rm ion}(n_0) \approx \sigma_{\rm ex}(n_0 - n_{\rm r}) , \qquad (70)$$

from Eqn (69) it follows that the electron-loss cross section of ions in a dense medium is roughly two times higher than that in the low-density medium. Let us recall that, under the conditions of electron capture, the density effects lead to much significant change in the cross section — to its reduction by more than 10-fold.

The mutual change in electron loss and capture cross sections, considered above, gives a qualitative explanation of increasing the equilibrium mean charge for ion beams passing through a dense medium. This statement is illustrated in Fig. 13, where the charge-changing cross sections are presented for heavy uranium ions penetrating through a dense plasma target (see Ref. [151]). The ion charges corresponding to the crossing points of the solid curves in

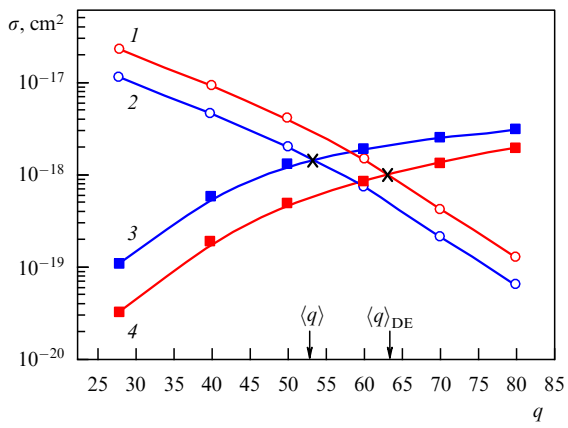


**Figure 13.** (Color online.) Electron-capture and electron-loss cross sections for 11-MeV/u uranium ions passing through a dense carbon plasma ($\rho = 5 \times 10^{19}$ cm$^{-3}$) as a function of uranium ion charge $q$ [151]. Curves *1* and *2* — electron-loss cross sections calculated with and without regard to density effects, respectively, and curves *4* and *3* — the same for electron-capture cross sections. Arrows indicate the equilibrium charges $\langle q \rangle_{\rm DE}$ and $\langle q \rangle$ obtained with and without regard to the density effects, respectively. The experimental value is $\langle q \rangle_{\rm exp} = 63 \pm 1$.

the figure are the equilibrium mean charges $\langle q \rangle$, i.e., when both processes are in equilibrium. Taking account of the density effects in calculations leads to an increase in the equilibrium mean charge and better agreement with experimental data.

Therefore, to describe the charge-changing processes occurring in a gas, plasma, or solid-state medium, the standard formulas for effective cross sections, generally speaking, cannot be applied, and one has to refer to formulas taking account of the density effects [see formulas (57), (62), and (63)].

## 6. Lifetimes of ion beams in accelerators

One of the main applications of the charge-changing cross sections is the determination of the lifetime $\tau$ for heavy-ion beams injected into an accelerator, where $\tau$ is defined by

$$I(t) = I_0 \exp\left(-\frac{t}{\tau}\right), \tag{71}$$

where $I_0$ denotes the initial intensity of the injected ion beam, and $I(t)$ is its time evolution. The lifetime $\tau$ depends on the so-called *vacuum conditions*, i.e., pressure and concentrations of the rest-gas components in the accelerator, and also on the ion energy and the charge-changing cross sections of beam ions colliding with the rest-gas atoms and molecules, usually being $H_2$, He, $O_2$, $N_2$, $H_2O$, CO, $CO_2$, $CH_4$, and Ar. For estimation of the vacuum conditions, the concentrations $Y$ of the 'reference' atoms and molecules ($H_2$, $N_2$, Ar) in accelerators are often used with the following magnitudes: $Y(H_2) \sim 70-90\%$, $Y(N_2) \sim 20-30\%$, and $Y(\mathrm{Ar}) \sim 1-3\%$.

For estimating the ion–beam lifetime in an accelerator, the following formula is commonly used:

$$\tau = \left[\rho\beta c \sum_{\mathrm{T}} Y_{\mathrm{T}}\big(\sigma_{\mathrm{EC}}(q, v, Z_{\mathrm{T}}) + \sigma_{\mathrm{EL}}(q, v, Z_{\mathrm{T}})\big)\right]^{-1}, \qquad \sum_{\mathrm{T}} Y_{\mathrm{T}} = 1\,, \tag{72}$$

where $\rho$ denotes the rest-gas density, $\beta = v/c$ is the relativistic factor, $q$ and $v$ are the charge and velocity of the projectiles, $Z_{\mathrm{T}}$ and $Y_{\mathrm{T}}$ are the nuclear charge and concentration of the rest-gas components, and $\sigma_{\mathrm{EC}}$ and $\sigma_{\mathrm{EL}}$ are the total, i.e., with account for multielectron processes, electron-capture and electron-loss cross sections of ion–target collisions.

In real conditions, the rest-gas density $\rho$ and concentrations $Y_{\mathrm{T}}$ take on different values in different points of the accelerator volume and are also time-dependent. Moreover, the rest-gas atoms and molecules can be ionized by the beam ions, leading to a change in their interactions with the projectiles, and to so-called *dynamic vacuum effects* arising in the accelerator at very high beam densities [42]. All these circumstances restrict the application of the beam lifetime (72) but, as a rule, it gives satisfactory results when estimating the ion-beam lifetimes in accelerators and storage rings.

As an example, experimental data on $U^{28+}$-ion beam lifetimes as a function of the ion energy at specified vacuum conditions are shown in Fig. 14 in comparison with theoretical calculations (see paper [76]); the vacuum parameters employed in calculations are indicated in the figure. In estimating the ion-beam lifetimes, the recommended cross sections given in Fig. 11 were used together with the

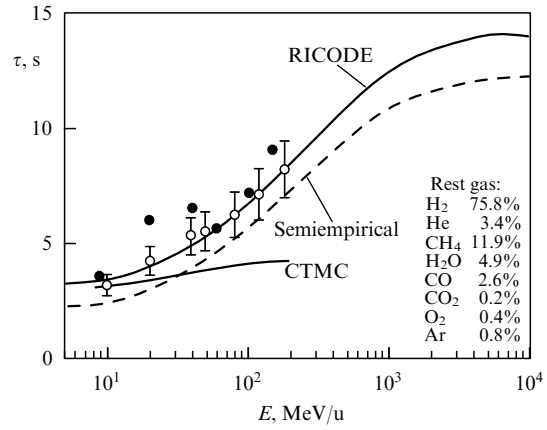


**Figure 14.** $U^{28+}$-ion beam lifetimes as a function of ion energy at a gas pressure in the vacuum chamber about $10^{-10}$ mbar and rest-gas concentrations shown in the figure. Experiment: black circles [152], and white circles [138]. Theory: the result of using formula (72) with electron-loss cross sections obtained with the CTMC code; RICODE — same but with electron-loss cross sections obtained with the RICODE program; dashed curve — obtained by using formula (72) with semiempirical formulas for electron-capture (12) and electron-loss (34) cross sections.

calculated results for C and O targets. The figure demonstrates quite the good agreement between theory and experiment conducted at the SIS18 synchrotron heavy-ion source in Darmstadt. We note that in the energy range considered, $E > 9$ MeV/u, the electron-capture cross sections of $U^{28+}$ ions colliding with the rest-gas atoms and molecules are negligible compared to electron-loss cross sections.

For relativistic energies, $E > 5$ GeV/u, the calculated lifetime of the uranium beam is predicted to be a constant of about 13 s for the vacuum parameters considered. From Fig. 14 it is also seen that the use of semiempirical formulas for electron-capture (12) and electron-loss (34) cross sections gives a reasonable estimate for the ion-beam lifetime over a wide energy range, including relativistic energies.

As appears from the above concerning formula (72), the ion-beam lifetime in accelerators depends on the vacuum parameters and charge-changing cross sections of ions. In practice, however, simultaneous measurements of ion-beam lifetimes and residual-gas density and concentrations is a difficult problem, but one can turn to solving the inverse problem — now to estimate the vacuum conditions from ion lifetimes and charge-changing cross sections known from theory or experiment.

The 11.4-MeV/u $U^{q+}$-ion beam lifetimes $\tau$ as a function of the ion charge $q$ are presented in Fig. 15. Experimental data on $\tau$ were obtained at the SIS18 heavy-ion synchrotron, Darmstadt, for charges $q = 34-42$, but the vacuum conditions were not known properly (see report [153]). Utilizing the charge-changing cross sections of uranium ions calculated by the CAPTURE, DEPOSIT, and RICODE programs, and experimental data on $\tau$, the estimated vacuum parameters were found: $\rho = 1.5 \times 10^{-10}$ mbar, $Y(H_2) \approx 75\%$, $Y(N_2) \approx 24\%$, and $Y(\mathrm{Ar}) \approx 1\%$, i.e., a good agreement with experimental ion-beam lifetimes was reached with these vacuum parameters and cross sections. The vacuum parameters obtained this way are close to expected parameters at the SIS18 synchrotron ion source. Here, the key role of electron capture processes at the ion energy $E = 11.4$ MeV/u considered should be noted: their inclusion leads to a decrease in

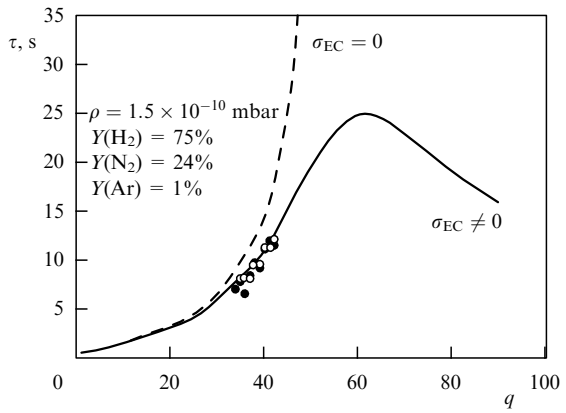


**Figure 15.** 11.4-MeV/u $U^{q+}$-ion beam lifetimes as a function of the ion charge $q$. Experiment: white and black circles — SIS18 data, Darmstadt [153]. Theory: dashed curve was calculated with electron-capture processes neglected, and solid curve was calculated with both electron-capture and electron-loss processes included. The vacuum parameters employed in the calculations are indicated in the figure.

the ion-beam lifetimes for uranium ions with charges $q > 60$, and neglecting the capture processes causes an infinite increase in $\tau$ with increasing ion charge. Therefore, the uranium $U^{q+}$ ions with charges $q \approx 60$ are the best candidates for detection of the longest ion-beam lifetime $\tau \approx 25$ s at the energy $E = 11.4$ MeV/u.

Certainly, the solution of the inverse problem considered here is not unambiguous, but the procedure for estimation of the vacuum parameters may be useful for interpretation of experimental data and planning future experiments with heavy many-electron ion beams in accelerator facilities.

## 7. Charge exchange in slow collisions

In this chapter, charge-exchange process in slow ion–atom collisions are considered, where the collision velocities are small, $v \ll 1$ a.u., and the motion of nuclei can be treated classically. Slow collisions are of special interest, both from the experimental (processes in low-temperature plasmas) and theoretical points of view. A characteristic feature of slow collisions is the formation of quasimolecules, while the internuclear distance between the interacting particles is decreasing. The study of the mechanisms and probabilities of electron transitions in such collisions has resulted in the development of new theoretical approaches and methods. The most common is the *adiabatic approximation* based on an approximate separation of the 'fast' (electron motion) and 'slow' (motion of nuclei) variables of a dynamical system.

The fundamentals of the adiabatic approximation — the approximate separation of the electronic, vibrational, and rotational degrees of freedom in molecules, and the solution of the nonstationary Schrödinger equation with the Hamiltonian slowly changing in time — were laid in Refs [154, 155]. Investigations of the probability of nonadiabatic transitions have been performed in several papers using different theoretical approaches [156, 157], solving model problems [158], and considering the quantum motion of interacting particles [159].

The development and application of the adiabatic approach for the calculation of the excitation, charge exchange, and ionization cross sections in slow atom–atom and atom–molecule collisions have been the subject of several monographs and reviews [2, 160–164]. The growing interest in slow ion–atom collisions due to creating installations with magnetic plasma confinement has led to a number of studies [165–169] where exactly solvable models were considered. These models allowed exploring a large number of specific physically important processes and creating the *theory of adiabatic transitions in slow collisions*, which treats them as standard problems [13, 170].

In this article, the charge exchange process is considered in the framework of the adiabatic theory [13, 170], where the transitions between electronic states of colliding particles are described by the nonstationary Schrödinger equation in the classical approximation to nuclei motion:

$$H(\mathbf{R})\,\psi(\mathbf{r},t) = \mathrm{i}\,\frac{\partial\psi(\mathbf{r},t)}{\partial t}\,,$$

where $\mathbf{r}$ is a set of electron coordinates, and $H(\mathbf{R})$ is the electronic Hamiltonian of a diatomic quasimolecule, depending on time only through internuclear distance $\mathbf{R} = \mathbf{R}(vt)$ ($v$ is the relative velocity of the nuclei), which is a known function of time.

In the most common form, the adiabatic approximation comprises an asymptotic expansion of the solution to the nonstationary Schrödinger equation in a small parameter $v$. In this approximation, the electron wave function is sought for in the form of the expansion

$$\psi(\mathbf{r},t) = \sum_{\mathrm{p}} g_{\mathrm{p}}(t)\,\varphi_{\mathrm{p}}(\mathbf{r},R)\exp\left(-\mathrm{i}\int^{t} E_{\mathrm{p}}\big(R(vt')\big)\,\mathrm{d}t'\right)$$

in the eigenfunctions $\varphi_{\mathrm{p}}$ of the instantaneous electronic Hamiltonian

$$H(\mathbf{R})\,\varphi_{\mathrm{p}}(\mathbf{r},R) = E_{\mathrm{p}}(R)\,\varphi_{\mathrm{p}}(\mathbf{r},R)\,,$$

which depend on $R$ as on the parameter entering into Hamiltonian. The eigenvalues $E_{\mathrm{p}}(R)$ have several names in the physics of atomic collisions: molecular potential curves, adiabatic potential curves, or simply potential curves. In this representation, the adiabatic approximation is reduced to the calculation of the leading terms of the expansion coefficients $g_{\mathrm{p}}(t)$ when $v \to 0$.

The ARSENY code was created for numerical calculation of the charge exchange cross sections [171]. This code is based on the method of hidden crossings of the electronic potential curves, which are the eigenvalues of the two-center Coulomb problem [172]. Along with the hidden crossings method, programs that are based on the close coupling methods [173–178], the electron nuclear dynamics [179], and the solution of the three-body Coulomb problem [180] are also used for calculating the charge exchange cross sections in slow collisions.

In low-temperature plasmas (edge plasma and plasma in a divertor of tokamaks and stellarators), charge exchange is the dominant process in the population of the excited states of the plasma ions and, therefore, plays an important role in ion charge distribution, radiative cooling, and the transport of particles. Experiments on cold plasma diagnostics have shown that the simulation of such a plasma needs consideration of the resonant charge exchange (RCE) between highly excited states of the plasma particles (H, He) and plasma impurities (Li, Be, C, W) [181, 182], which requires development of the theory of RCE between excited states. Such a theory was developed for slow collisions of protons with

excited hydrogen atoms, since the state of an arbitrary atom with one excited outer-shell electron can be approximately described in the hydrogen approximation with an effective charge of the atomic core.

Below, two processes are considered in detail: the resonant charge exchange in slow collisions of protons with hydrogen atoms in the excited state, and the charge exchange between heavy ions and hydrogen isotopes. These processes have been selected for a detailed description because of the novelty of the theoretical approach to calculating the RCE cross sections and of the effect which occurs in reactions involving hydrogen isotopes H, D, and T.

### 7.1 Resonant charge exchange between protons and hydrogen atoms

In this section, the RCE in slow collisions (the center-of-mass energy $E \leqslant 1$ a.u. $\approx 27.202$ eV) of a proton with an excited hydrogen atom is discussed. Recent experiments on cold plasma diagnostics have shown the necessity of including the RCE between excited states in plasma simulations [179, 180]. RCE between the ground (initial and final) states of the hydrogen atom in slow collisions is described by the Firsov–Demkov theory [165, 183] and has been well studied theoretically [175, 184, 185]. However, this theory does not apply to describing excited states, due to their degeneration. Indeed, there is now a limited amount of data for RCE cross sections involving excited degenerate states, which were calculated by the close coupling method [173, 174], while for energies below 1 a.u. there is virtually no data.

The theory of RCE between excited states, which is an extension of the Firsov–Demkov theory to the case of degenerate initial and final states, was first developed and described in paper [186]. On the basis of this theory, the RCE computer code (Resonant Charge Exchange) was created, and the charge exchange cross sections for energies of less than 1 a.u. were obtained initially for the reaction

$$\mathrm{H}(n=2) + \mathrm{H}^+ \to \mathrm{H}^+ + \mathrm{H}(n=2)\,. \tag{73}$$

**7.1.1 Resonant charge exchange in p–H collisions involving ground-state hydrogen atoms.** To illustrate the reliability of the suggested method of calculating the RCE cross sections between degenerate excited states, we start from the well-known case of $n = 1$ and compare the results obtained with available data. The method aimed at calculating the RCE cross sections for the reaction

$$\mathrm{H}(n=1) + \mathrm{H}^+ \to \mathrm{H}^+ + \mathrm{H}(n=1) \tag{74}$$

at low collision energies was developed by Firsov [183]. His theory gives the following semiclassical expression for the RCE cross section:

$$\sigma = 2\pi \int_0^\infty \sin^2\left(\int_b^\infty \frac{E_\mathrm{g}(R) - E_\mathrm{u}(R)}{2v\sqrt{R^2 - b^2}}\, R\,\mathrm{d}R\right) b\,\mathrm{d}b\,, \tag{75}$$

where $R$ is the internuclear distance, $b$ is the impact parameter, $v$ is the relative velocity, and $E_\mathrm{g}(R)$ and $E_\mathrm{u}(R)$ are the electron energies (eigenvalues of the two-center Coulomb problem [172]) corresponding to gerade (even) and ungerade (odd) states shown in Fig. 16a. Parity of the electronic state described by spheroidal quantum numbers $n_\eta$, $n_\zeta$, and $m$ is defined as $(-1)^{n_\eta}$ [172].

Firsov's theory provides a method for calculating the RCE, but does not describe the mechanism of electron transition. Demkov considered the more general problem of quasi-resonance charge exchange [165], when the energies of the initial and final states differ by a small value $\Delta E$. Using an exactly solvable Rosen–Zener model [187], he developed a theory which is widely applied in the physics of atomic collisions. In this theory, diabatic states correspond to the states of separated atoms, whereas adiabatic ones correspond to the molecular states. The adiabatic states coincide with the

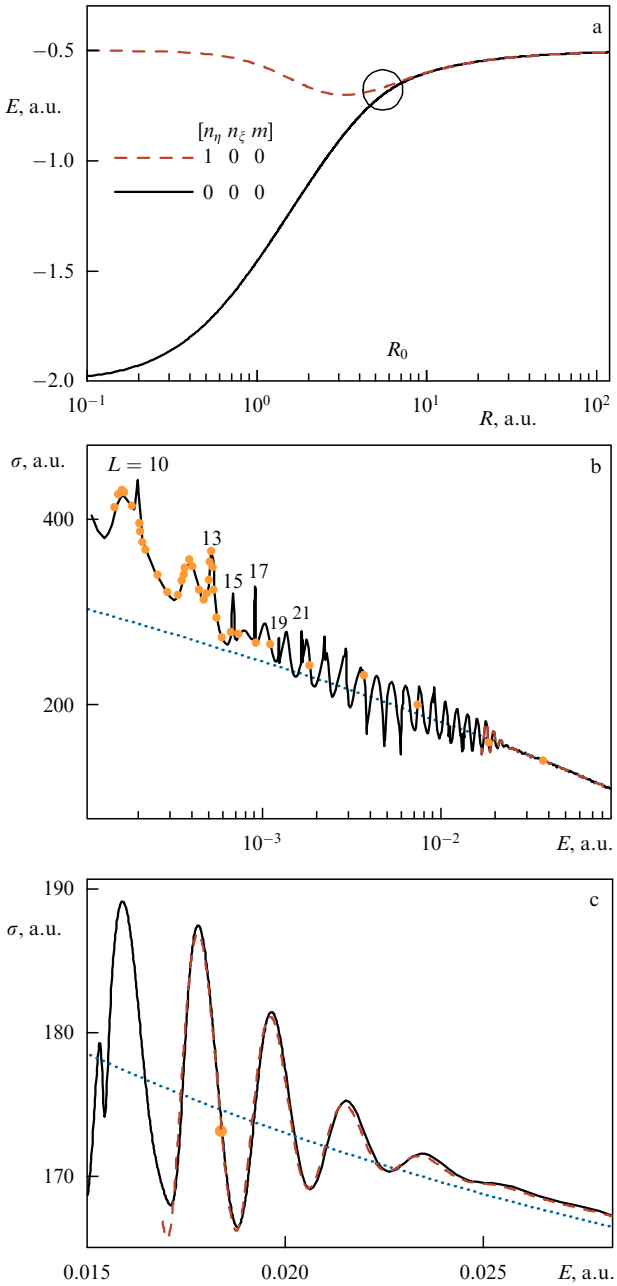


**Figure 16.** (Color online.) (a) Electron energies of the even (solid line) and the odd (dashed line) states participating in the RCE process $\mathrm{H}(n=1) + \mathrm{H}^+ \to \mathrm{H}^+ + \mathrm{H}(n=1)$ as a function of the internuclear distance. The electron charge exchange transition via the Demkov mechanism occurs in the circled region near the point $R_0$ defined by formula (76). (b, c) Cross sections of the RCE reaction $\mathrm{H}(n=1) + \mathrm{H}^+ \to \mathrm{H}^+ + \mathrm{H}(n=1)$ as a function of the center-of-mass collision energy: solid line — formula (77) with the quantum $\delta_{\mathrm{g,u}}(L)$; dashed line — formula (77) with quasiclassical $\delta_{\mathrm{g,u}}(L)$; dotted line — formula (75); dots — calculated results from Ref. [185]; region of convergence of quantum and quasiclassical calculations is shown in figure c in detail.

diabatic states as $R \to \infty$. The nonadiabatic interaction as a function of the internuclear distance has a maximum, when the diabatic (atomic) states rearrange into adiabatic (molecular) states. At this point in time, electron transition occurs. Thus, the Demkov theory describes the general mechanism of the charge exchange in the quasiresonance case. It is important to note that this theory in the limit of $\Delta E = 0$ gives a result coinciding with formula (75) obtained by Firsov [183].

Considering one-electron collision reaction (74) allows a much more advanced analysis, since the variables of the two-center Coulomb problem are separable in the prolate spheroidal coordinates [172]. The adiabatic theory of transitions in slow collisions in $Z_1 - e - Z_2$ electronic systems, where $Z_1$ and $Z_2$ are the effective charges of the nuclei, was developed by Solov'ev [13, 170]. It has been shown that in the quasiresonance case, $|1 - Z_1/Z_2| \ll 1$, corresponding to small values of $\Delta E$, the so-called P series of hidden crossings responsible for the Demkov mechanism exists [186]. The Solov'ev theory does not describe the RCE in symmetric systems with $Z_1 = Z_2$, since the even and the odd states in this case do not interact and there are no hidden crossings connecting the corresponding electron energy surfaces in the plane of complex $R$ values. Nevertheless, the Demkov theory is applicable to a more general class of collision systems describing the resonance case ($\Delta E = 0$), as well. Thus, in Ref. [186] it was concluded (this should be considered as a plausible assumption rather than a proven statement) that the transitions in the RCE process are localized in the regions where the atomic states rearrange into molecular ones. This happens near the point $R_0$, where the even and odd states become approximately degenerate. Using the semiclassical approximation [170], the $R_0$ value can be estimated from the following equation

$$R_0^2 E(R_0) + 2\lambda_{\mathrm{u}}(R_0) + 4\sqrt{\lambda_{\mathrm{u}}(R_0)} = 0\,, \tag{76}$$

where $E(R)$ and $\lambda_{\mathrm{u}}(R)$ are the electron energy and the separation constant for the odd state. In Fig. 16a, the region near the point $R_0$ for the case $n = 1$ is indicated by a circle.

Quantum representation of equation (75) has the following form [184, 185]:

$$\sigma = \frac{\pi}{(v\mu)^2} \sum_{L=0}^{\infty} (2L+1) \sin^2\left(\delta_{\mathrm{g}}(L) - \delta_{\mathrm{u}}(L)\right), \tag{77}$$

where $\delta_{\mathrm{g,u}}(L)$ is the scattering phase shift, $\mu$ is the reduced mass, and $L$ is the angular momentum associated with the internuclear axis. Starting from pioneering works [184] and [185], the RCE cross section for reaction (74) has been calculated using equation (77) and its energy dependence has been studied in detail (see, e.g., paper [175]). In this approach, the nuclei of the colliding particles (protons) were treated classically. To our knowledge, only one fully quantum calculation exists of the cross section for quasiresonance charge exchange between hydrogen atom in the ground state and deuteron, which is based on the solution of the three-body Coulomb problem [178].

In paper [186], the RCE cross sections for reaction (74) were calculated using the Firsov method in three different ways. The first one is semiclassical, and the cross section is defined by formula (75). The other two methods utilize formula (77), but the scattering phase shifts are calculated in different ways: in the quantum approach — by solving the stationary Schrödinger equation

$$\frac{\mathrm{d}^2}{\mathrm{d}r^2}\psi_{\mathrm{g,u}}(R) + \left[2\mu\left(\frac{1}{R} + E_{\mathrm{g,u}}(R) - \varepsilon_{\mathrm{cm}}\right) + \frac{L(L+1)}{R^2}\right] \times \psi_{\mathrm{g,u}}(R) = 0\,, \tag{78}$$

while in the semiclassical approach the scattering phase shifts are given by [189]

$$\delta_{\mathrm{g,u}}(L) = \int_{R_{\mathrm{t}}}^{\infty} \left[\sqrt{2\mu\left(\varepsilon_{\mathrm{cm}} - \frac{1}{R} - E_{\mathrm{g,u}}(R)\right) - \frac{(L+1/2)^2}{R^2}} - k\right] \mathrm{d}R + \frac{\pi}{2}\left(L + \frac{1}{2}\right) - kR_{\mathrm{t}}\,, \tag{79}$$

where $\mu$ is the reduced mass, $\varepsilon_{\mathrm{cm}}$ is the collision energy in the center-of-mass frame, $R_{\mathrm{t}}$ is the turning point, and $k = \sqrt{2\mu\varepsilon_{\mathrm{cm}}}$. The results of calculations [186] are shown in Fig. 16b, c.

The calculated results are converged with respect to all numerical parameters. A comparison of the calculated cross sections with the results presented in Ref. [185] (dots in Fig. 16b) shows good agreement over the whole energy range, except for small differences in the cross sections at low energies. This difference is due to the inclusion of nonadiabatic corrections to the potential [185]. The oscillations of the cross sections and positions of the orbiting resonances (the values of orbital momentum $L$ were ascribed to some of the resonances in Fig. 16b) are in very good agreement with the data reported in Refs [175] and [190]. Quantum calculations take a considerable time with an increase in energy, and a good convergence of the quantum results to quasiclassical ones (Fig. 16c) allows us to use the semiclassical $\delta_{\mathrm{g,u}}(L)$ for the RCE cross section calculations beginning from an energy of about 0.017 a.u. Cross sections evaluated with formula (75) (dotted line) do not reproduce the oscillatory structure and meet with the two others at a collision energy of about 1 a.u.

**7.1.2 Resonant charge exchange in p–H collisions involving hydrogen atoms in the excited $n = 2$ state.** As an example of RCE between excited degenerate states, we consider the following reaction

$$\mathrm{H}(n=2) + \mathrm{H}^+ \to \mathrm{H}^+ + \mathrm{H}(n=2)\,. \tag{80}$$

Figure 17a depicts the electron energies for six states converging to the $n = 2$ level in the limit of the far removed atoms ($R \to \infty$), which are relevant for a discussion of this reaction. In the limit of separated atoms, the principal quantum number $n$ is expressed in terms of spheroidal quantum numbers $n_\eta$, $n_\xi$, and $m$ of the electronic state as follows:

$$n = n_\xi + \left[\frac{n_\eta}{2}\right] + m + 1\,, \tag{81}$$

where $[a]$ denotes the integer part of $a$. In this limit, the spheroidal coordinates are transformed into parabolic coordinates, and the correspondence between spheroidal $(n_\eta, n_\xi, m)$ and parabolic $(n_1, n_2, m)$ quantum numbers is given by the formulas [172]

$$n_1 = n_\xi\,, \qquad n_2 = \left[\frac{n_\eta}{2}\right]. \tag{82}$$

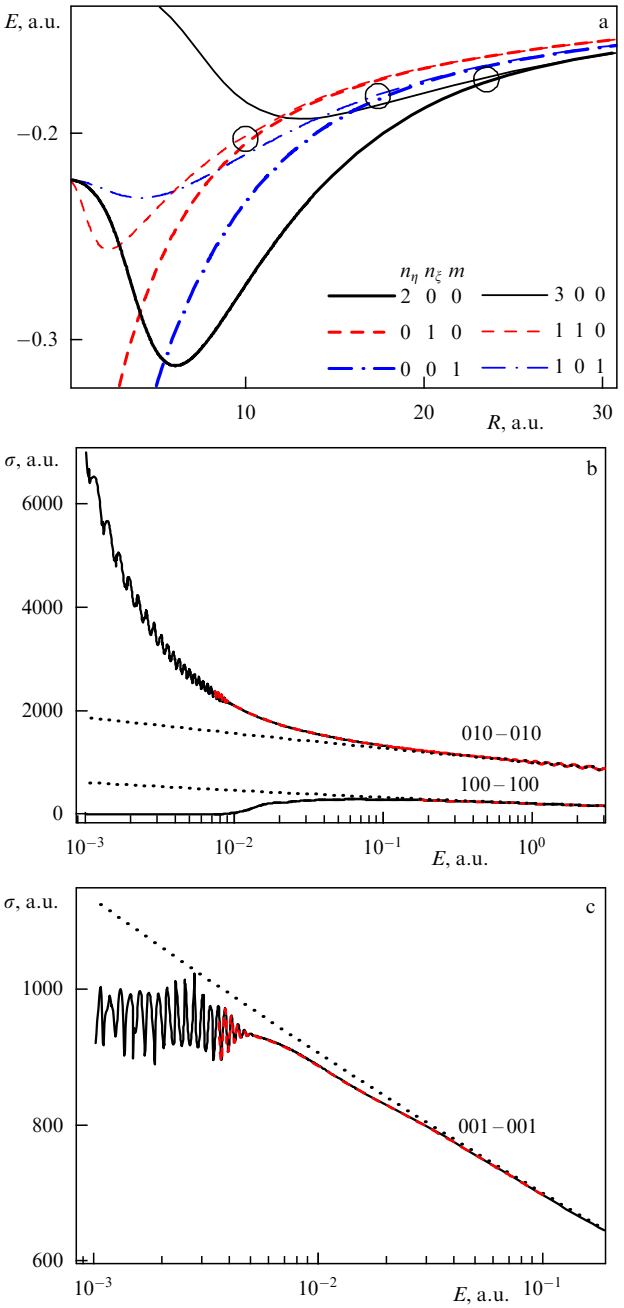


**Figure 17.** (Color online.) (a) Electron energies of the even (thick lines) and odd (thin lines) states participating in the RCE reaction $\mathrm{H}(n=2)+\mathrm{H}^+\to\mathrm{H}^++\mathrm{H}(n=2)$ as a function of the internuclear distance. Electron transitions due to the Demkov mechanism occur in the circled regions defined by formula (76). (b, c) RCE cross sections of the reaction $\mathrm{H}(n_1,n_2,m)+\mathrm{H}^+\to\mathrm{H}^++\mathrm{H}(n_1,n_2,m)$ as a function of the center-of-mass collision energy for parabolic states 010 (b), 100 (b), and 001 (c): solid lines — formula (77) with the quantum $\delta_{\mathrm{g,u}}(L)$; dashed lines — formula (77) with quasiclassical $\delta_{\mathrm{g,u}}(L)$; dotted lines — formula (75).

First of all, we note that the electronic states displayed in Fig. 17a can be divided into three pairs each consisting of even and odd states with the same values of $n_\xi$ and $m$. Within each pair, the $n_\eta$ value of the odd state exceeds $n_\eta$ of the even state by unity; hence, both states are described by the same set of parabolic quantum numbers $n_1$, $n_2$, and $m$ as $R\to\infty$. It should be noticed that the degeneracy within the pair occurs at much smaller internuclear distances than that between pairs. In what follows, such a pair of states will be called degenerate. In Fig. 17a, the states belonging to the same degenerate pair are shown by the same line style.

The approach to the calculation of the RCE cross section in reaction (80) is as follows: electron transitions within the degenerate pairs are treated applying the Firsov–Demkov theory, while the interaction between different pairs converging to the level with $n=2$, as well as their interaction with states converging to the different $n$-states, are neglected. In the adiabatic approximation (slow collisions), this approach is justified by the fact that the regions of localized electron transitions in degenerate pairs (circles in Fig. 17a), described by the Demkov mechanism, are separated well by the internuclear distance. A similar approach found application in Ref. [191] for calculations of the cross sections of quasiresonant charge exchange between the $n=2$ states, where the Demkov interaction inside each pair of quasidegenerate states was taken into account, and all other interactions were neglected. The results obtained in Ref. [191] are in good agreement with the available exact quantum results [192], where the same three-body Coulomb system was considered. This fact offers an additional independent argument supporting the present approach.

RCE cross sections between parabolic states with $n=2$ and $m=0$ and 1 are plotted in Fig. 17b, c. Cross sections corresponding to electron transitions between parabolic 010 – 010 and 001 – 001 states reveal a resonance structure and increase as the collision energy decreases, whereas the cross section of the 100 – 100 transition does not have resonances and decreases. Figure 18a demonstrates the potentials

$$U(R)=\frac{1}{n^2}+\frac{1}{R}+E_{\mathrm{g,u}}(R)$$

for the three pairs of spheroidal states. It can be seen from the figure that the potentials of the 010 and 110 states are repulsive. The turning point $R_{\mathrm{t}}$ [internuclear distance whereat the argument of the square root in formula (79) becomes zero] moves to the right as the energy decreases. When $R_{\mathrm{t}}$ becomes larger than 10 a.u. ($R_0$ for these states), which happens at an energy of about 0.02 a.u., the cross section decreases rapidly, as is evidenced in Fig. 17b. Several resonances in the transition between parabolic states 010 – 010 and the corresponding orbital momenta $L$ are also indicated in Fig. 18b.

The potentials of the form

$$U(R)=\frac{1}{n^2}+\frac{1}{R}+E_{\mathrm{g,u}}(R)+\frac{L(L+1)}{2\mu R^2}$$

for the spheroidal 200 and 300 states and the orbital momentum $L=90$ are plotted in the inset. In the potential of the 200 state there is a barrier which causes the first orbital resonance in Fig. 18b. Since the collision energy $E_{L=90}$ corresponding to this resonance is very close to the top of the barrier, the resonance width is quite large. We studied the convergence of the RCE cross sections between parabolic 010 – 010 states calculated using formula (77) with the quantum and semiclassical phase shifts $\delta_{\mathrm{g,u}}(L)$, and the convergence of the cross sections defined by formulas (75) and (77). Analysis of the results leads to the following conclusion: it is possible to calculate the RCE cross sections using formula (77) with the semiclassical phase shifts $\delta_{\mathrm{g,u}}(L)$, starting from a collision energy of about 0.008 a.u., and to apply formula (75) from 2 a.u.

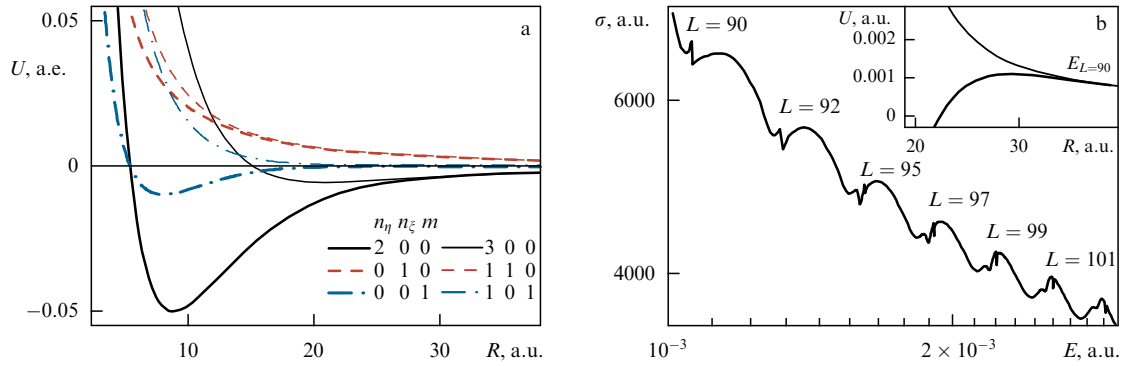


**Figure 18.** (Color online.) (a) Potentials $U(R) = 1/n^2 + 1/R + E_{\mathrm{g,u}}(R)$ for the even and odd spheroidal states as a function of internuclear distance. (b) Orbital resonances in the RCE cross sections as a function of the center-of-mass collision energy for parabolic 010−010 states. Inset: potentials $U(R) = 1/n^2 + 1/R + E_{\mathrm{g,u}}(R) + L(L+1)/(2\mu R^2)$ for spheroidal 200 (thick line) and 300 (thin line) states for the orbital momentum $L = 90$ as a function of the internuclear distance.

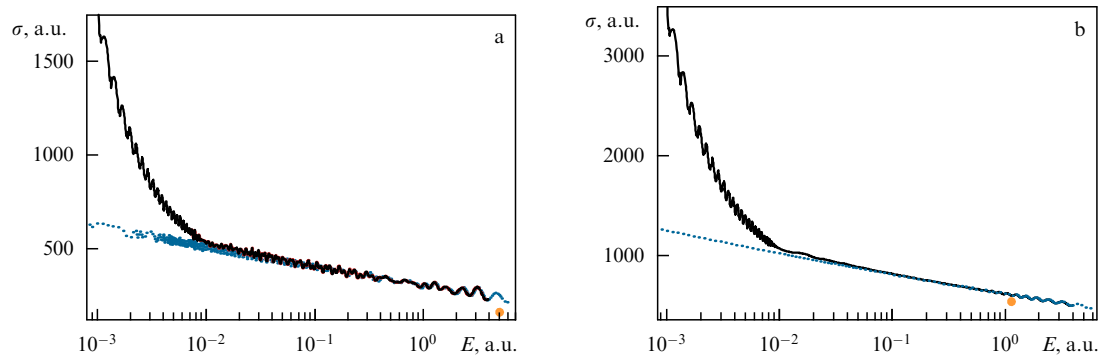


**Figure 19.** (Color online.) (a) RCE cross sections of the $\mathrm{H}(n,l,m) + \mathrm{H}^+ \to \mathrm{H}^+ + \mathrm{H}(n,l,m)$ reaction as a function of the center-of-mass collision energy for the spherical 2s0 and 2p0 states: solid line — formula (77) with the quantum $\delta_{\mathrm{g,u}}(L)$; dashed line — formula (77) with quasiclassical $\delta_{\mathrm{g,u}}(L)$; dotted line — formula (75); dot — result from Ref. [173]. (b) Total RCE cross section of the $\mathrm{H}(2s0) + \mathrm{H}^+ \to \mathrm{H}^+ + \mathrm{H}(2s0, 2p0)$ reaction as a function of the center-of-mass collision energy for the spherical 2s0 and 2p0 states: solid line — formula (77), dotted line — formula (75); dot — result from Ref. [174].

The transformation from parabolic to spherical coordinates is accomplished by utilizing the Clebsch–Gordan coefficients [189]. The RCE cross section between spherical $nlm-nl'm$ states can be represented as follows:

$$\sigma_{nlm-nl'm}(v) = \frac{\pi}{(v\mu)^2} \sum_{L=0}^{\infty} (2L+1) \times \left| \sum_{n_1 n_2 m} c(n_1 n_2 m - nlm) A_{n_1 n_2 m}(L)\, c(n_1 n_2 m - nl'm) \right|^2, \quad (83)$$

where

$$A_{n_1 n_2 m}(L) = \sin\left[\delta_{\mathrm{g}}(L) - \delta_{\mathrm{u}}(L)\right] \exp\left[\mathrm{i}\left(\delta_{\mathrm{g}}(L) + \delta_{\mathrm{u}}(L)\right)\right] \quad (84)$$

is the RCE amplitude in parabolic coordinates, and

$$c(n_1 n_2 m - nlm) = (-1)^{n_1+m} \sqrt{2l+1} \times \begin{pmatrix} \dfrac{n-1}{2} & \dfrac{n-1}{2} & l \\ \dfrac{n_2 - n_1 + m}{2} & \dfrac{n_1 - n_2 + m}{2} & -m \end{pmatrix}. \quad (85)$$

The second summation in expression (83) is performed over parabolic states with the same quantum numbers $n$ and $m$. As a result, we obtain RCE cross sections for the following transitions: 2s0−2s0, 2p0−2p0, 2p0−2s0, and 2p1−2p1. Because of the properties of the Clebsch–Gordan coefficients, the cross sections of 2s0−2s0 and 2p0−2p0 transitions are equal; they are displayed in Fig. 19a. The point in the figure marks the cross section of the 2s0−2s0 transition at velocity $v = 0.1$ a.u., calculated by the semiclassical close-coupling method [173]. The difference of about 30% between present calculations and the data from Ref. [173] can be explained by the fact that our method does not take into consideration some other processes (nonresonant charge exchange, excitation, and ionization), whose probabilities become significant with an increase in the collision energy.

The cross sections of 2s0−2s0 and 2s0−2p0 transitions are displayed in Fig. 19b. The results are compared with the total cross section of the transition from the 2s0 state at a collision velocity of 0.05 a.u., which was calculated in the molecular close-coupling approach [174]. The difference of 9% means that at this velocity the contribution from the processes, which we do not account for, decreases in comparison to their contribution at a collision velocity of 0.1 a.u. As far as we know, there are no other data for the energy range considered. The RCE cross section of the 2p1−2p1 transition (Fig. 17c) does not change during the transformation from parabolic to spherical coordinates.

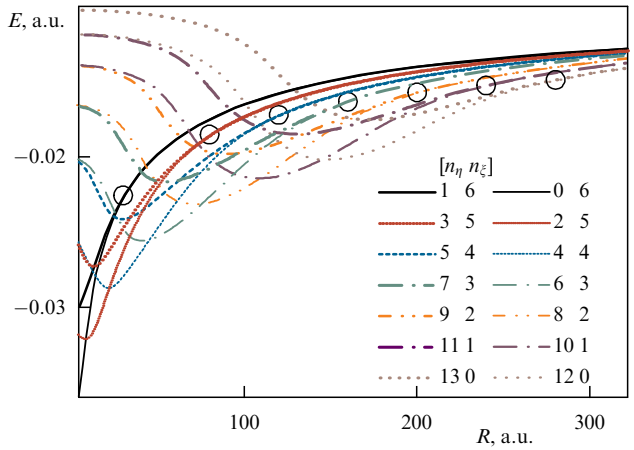


**Figure 20.** (Color online.) Electron energies of the even and odd states participating in the RCE process $\mathrm{H}(n=7, m=0)+\mathrm{H}^+ \to \mathrm{H}^+ + \mathrm{H}(n=7, m=0)$ as a function of the internuclear distance. Electron transitions due to the Demkov mechanism occur in the circled regions defined by formula (76).

Figure 20 illustrates the validity of the theory, developed in work [186] for the case of $n=2$ states, for an arbitrary excited state. This figure shows the electron energies of the excited degenerate states of atomic hydrogen in the following RCE process:

$$\mathrm{H}(n=7, m=0)+\mathrm{H}^+ \to \mathrm{H}^+ + \mathrm{H}(n=7, m=0)\,. \quad (86)$$

As is seen from the figure, the system of 14 electronic states is split into 7 pairs of even and odd states, and the regions of transitions within each degenerate pair (circles in the figure) are well separated by the internuclear distance. This means that the approach proposed can find application at collision energies such that the processes due to the interaction between pairs may be neglected.

### 7.2 Isotope effects in charge exchange reactions involving hydrogen isotopes

In this section, we consider the influence of the isotope effect (mass dependence) on the charge exchange process in slow collisions of Li, C, and W ions (materials used for plasma facing components in fusion devices) with hydrogen isotopes (H, D, and T). The isotope effect is studied in the framework of the adiabatic theory of electron transitions in slow collisions [13, 170]. Numerical results are presented below for the probabilities and the cross sections of charge exchange of Li, C, and W ions colliding with hydrogen isotopes, and for the reverse reaction.

**7.2.1 Mechanism of the isotope effect in slow collisions.** The isotope effect was first observed in collisions of alpha particles ($\mathrm{He}^{2+}$) with H, D, and T atoms at very low energies $E=1-500$ eV/u [193]. This effect is due to the rotational mixing of the electronic states at small internuclear distances $R$. Rotational interaction mixes the pairs of electronic states with the same principal and orbital quantum numbers $n$ and $l$, with the same parity, and with magnetic quantum numbers differing by unity ($\Delta m=\pm 1$). The amplitude of the $m$-changing transition caused by rotational interaction depends on the trajectory of the colliding particles, which, in turn, depends on their reduced masses: the heavier the isotope, the larger the charge-exchange cross section.

Nonadiabatic transitions caused by rotational interaction between quasimolecular states degenerate in the united atom limit ($R=0$) are of interest from a theoretical point of view, since they constitute non-Landau–Zener type transitions [13, 170]. The influence of the rotational coupling on the charge-exchange cross sections in slow collisions was studied in Ref. [193] for the $\mathrm{He}^{2+}+\mathrm{H}(1\mathrm{s})$ reaction. It was revealed that for collision energies below 1 keV/u the main contribution to the charge-exchange cross section is made by transitions caused by the rotational interaction in close collisions.

A strong isotope effect due to rotational interaction was observed and studied in Refs [193, 195, 196] for $\mathrm{He}^{2+}+\mathrm{H}, \mathrm{D}, \mathrm{T}$ processes which are of considerable interest for plasma modeling in fusion devices. These studies fell back on the Electron Nuclear Dynamics (END) approach [179] based on the solution of the time-dependent Schrödinger equation, with the trajectories of heavy particles determined by a scattering potential that evolves in accordance with the dynamics of the electrons.

The influence of the isotope effect on the charge exchange in slow collisions of Li, C, and W ions with H, D, and T isotopes was studied in Refs [197, 198] in the framework of the adiabatic theory based on the method of hidden crossings [13, 170]. The charge exchange process plays a key role in the transport of the particles and forming the charge distribution of the impurities in D–T plasmas. In the theory of ion–atom collisions, the adiabatic approximation is employed to describe electron transitions, when the particle collision velocity is small and the nuclear motion can be treated classically. In this theory there are no assumptions of the specific form of the electronic Hamiltonian, and only the smallness of the relative nuclear velocity finds use. This results in a deeper understanding of the nature of nonadiabatic transitions.

Since the isotope effect shows itself at collision energies where the adiabatic theory is applicable, the adiabatic approximation is a natural theoretical tool for studying the isotope effect. Numerical calculations of the charge exchange probabilities and cross sections were performed using the ARSENY computer code [171] based on the adiabatic approximation. To find the amplitude of the $m$-changing transition caused by the rotational interaction, the nonstationary Schrödinger equation with the Coulomb nuclear trajectory in the united atom limit was solved numerically.

**7.2.2 Calculations of the charge-exchange cross sections in the adiabatic approximation.** To illustrate the applicability of the adiabatic approach [197], let us consider the reaction

$$\mathrm{Li}^{3+}+\mathrm{H}(\mathrm{D},\mathrm{T})(1\mathrm{s}) \to \mathrm{Li}^{2+}(nl)+\mathrm{H}(\mathrm{D},\mathrm{T})^+\,. \quad (87)$$

Figure 21a gives the energies of the electronic states for reaction (87). These energies are the eigenvalues of the two-center Coulomb problem [172], which is separable in the longitudinal spheroidal coordinates and in our approach is solved for the complex internuclear distance. In Fig. 21a, the quasimolecular states are described by the spherical quantum numbers of the united atom. In the adiabatic theory, the charge exchange transitions occur at internuclear distances where the electron wave function changes rapidly. This happens when the nonadiabatic interaction reaches its maximum.

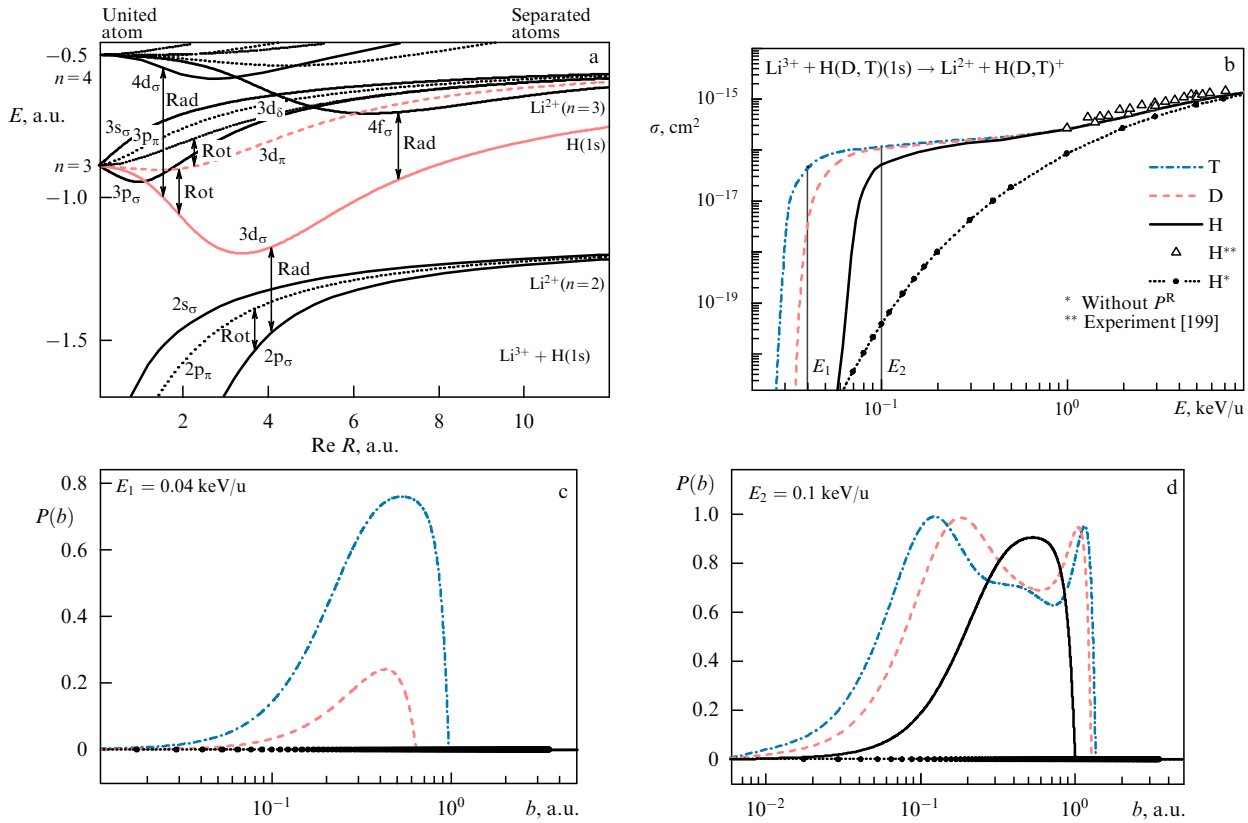


**Figure 21.** (Color online.) (a) Potential curves describing the charge exchange process $Li^{3+} + H(D,T)(1s) \to Li^{2+}(nl) + H(D,T)^{+}$ as a function of the internuclear distance (see text). (b) Total charge-exchange cross sections as a function of collision energy. (c, d) Probability of the transition as a function of the impact parameter, calculated with and without regard for rotational interaction $P^{R}$ for the reaction $Li^{3+} + H(D,T)(1s)$. Types of curves are illustrated in figure b.

Charge exchange transitions caused by radial coupling occur in the hidden crossings (branching points) at complex internuclear distances $R$, where the electronic energies of two states are equal. The hidden crossings arise when the system passes the state corresponding to the unstable periodic orbit. Hidden crossings are invisible on the plot of the adiabatic potential curves at real values of the adiabatic parameter $R$ (internuclear distance) and require direct calculations in the complex $R$ plane.

These 'radial' transitions are indicated in Fig. 21a by arrows Rad which connect the initial [H(1s) in the separated atom limit] and the final states of the electron, and are located at real $R$ values of the corresponding hidden crossings. Three transitions of this kind occur at internuclear distances 1.5, 4, and 7 a.u. (we consider the resonance channel $Li^{3+} + H(1s) \to Li^{2+}(n = 3) + H^{+}$ responsible for the isotope effect). The electron transition occurring at $\mathrm{Re}\, R = 1.5$ a.u. does not contribute to the process of charge exchange, since the corresponding hidden crossing belongs to S series (called 'superpromotion' of the diabatic term to a continuum [13, 170]). This interaction couples pairs of electronic states $E_{nlm}(R)$ and $E_{n+1\,lm}(R)$ and leads to emerging an ionization process in the adiabatic approximation. The other two transitions lead to a change in the charge state, and the transition between $3d_\sigma$ and $4f_\sigma$ states comprises the main radial transition in the resonance channel.

Rotational interaction associated with the internuclear axis rotation in close collisions induces transitions between $E_{nlm}(R)$ and $E_{nlm\pm1}(R)$ electronic states degenerate in the united atom limit. The potential curves of these states have the exact crossing at complex values of $R$ ($\mathrm{Re}\, R = 0$). In Fig. 21a, these transitions are indicated by arrows Rot located at arbitrary values of $R$. Rotational transition $3d_\sigma - 3d_\pi$ is the transition that causes the isotope effect in reaction (87).

To calculate the RCE cross sections, the ARSENY code based on the hidden-crossing method was applied [171]. In the adiabatic approximation, radial inelastic transitions occur in the regions of the closest approach of the potential curves and are decomposed into a sequence of individual two-level transitions through hidden crossings. First, adiabatic potential curves as a solution of the two-center Coulomb problem in the complex $R$ plane are found. Then, the code finds all branching points and calculates the appropriate Stueckelberg parameters

$$\Delta_{pq} = \left| \mathrm{Im} \int_{\mathrm{Re}\, R_c}^{R_c} \left[ E_p(R) - E_q(R) \right] \frac{\mathrm{d}R}{v(R,b)} \right| , \qquad (88)$$

where $p$ and $q$ comprise the set of quantum numbers, $E_p$ and $E_q$ are the energies of the initial and final states of the active electron, $R_c$ is a complex branching point, $v(R,b)$ is the radial internuclear velocity, and $b$ is the impact parameter.

Transition probability $P_{pq}$ as a function of the impact parameter is calculated for the entire set of nonadiabatic transitions as follows:

$$P_{pq} = \exp\left(-2\Delta_{pq}\right) . \qquad (89)$$

Then, the $S$-matrix is evaluated as the product of elementary $S$-matrices for individual transitions induced by various branching points. Starting with the initial $S$-matrix $S_{ij}^{(n)} = \delta_{ij}$, a change in the $S$-matrix due to the $n$th transition between $p$ and $q$ states, induced by the branching point at internuclear distance $R_c$, is defined in the following way:

$$S_{ip}^{(n)} = S_{ip}^{(n-1)}(1 - P_{pq}) + S_{iq}^{(n-1)} P_{pq}\,, \tag{90}$$

$$S_{iq}^{(n)} = S_{iq}^{(n-1)}(1 - P_{pq}) + S_{ip}^{(n-1)} P_{pq}\,. \tag{91}$$

Integrating the $S$-matrix over the impact parameter, we finally obtain a complete set of charge-exchange cross sections between arbitrary initial and final states, namely

$$\sigma_{qq} = 2\pi \int_0^\infty |1 - S_{qq}|^2 b\,\mathrm{d}b \tag{92}$$

for elastic scattering, and

$$\sigma_{pq} = 2\pi \int_0^\infty |S_{pq}|^2 b\,\mathrm{d}b \tag{93}$$

for an inelastic transition, where $S_{pq}$ are the elements of the $S$-matrix. To find the amplitude of the $m$-changing transition caused by the rotational interaction, the time-dependent Schrödinger equation was solved numerically for the Coulomb nucleus trajectory in the united atom approximation. Rotational interaction is taken into consideration if the following condition is satisfied: the internuclear separation should be less than

$$R_{\max} = \frac{(l + 1/2)^2}{Z_1 + Z_2}\,, \tag{94}$$

where $l$ is the orbital angular momentum of the electron, and $Z_1$ and $Z_2$ are the nuclear charges. This condition defines the boundary of the united atom region. Since the scattering angle

$$\chi = 2\arctan \frac{Z_1 Z_2}{\mu b v^2} \tag{95}$$

depends on the reduced mass $\mu$, the mechanical trajectories of the heavy particles in the reactions with H, D, and T are different. This, in turn, leads to a difference in the corresponding charge-exchange cross sections. The amplitude of the rotational transition is the solution of the time-dependent Schrödinger equation ($b < R_{\max}$ and $R_{\max} > R_{\mathrm{clmb}}$, where $R_{\mathrm{clmb}}$ is the internuclear separation corresponding to the closest approach):

$$\mathrm{i}\dot{a}_m - E_m a_m + \mathrm{i} \sum_{m'=-l}^{l} \left\langle \varphi_{nlm} \middle| \frac{\partial}{\partial t} \middle| \varphi_{nlm'} \right\rangle a_{m'} = 0\,. \tag{96}$$

Here, the following notation was introduced:

$$E_m = 3Dm^2R^2\,, \tag{97}$$

$$D = \frac{Z_1 Z_2 (Z_1 + Z_2)^2}{n^3 l(l+1)(2l-1)(2l+1)(2l+3)}\,, \tag{98}$$

$$\sum_{m'=-l}^{l} \left\langle \varphi_{nlm} \middle| \frac{\partial}{\partial t} \middle| \varphi_{nlm'} \right\rangle = \frac{1}{2}\frac{\partial \varphi}{\partial t}\left[\sqrt{(l+m)(l-m+1)}\,\delta_{m',m-1} + \sqrt{(l-m)(l+m+1)}\,\delta_{m',m+1}\right], \tag{99}$$

where $\varphi_{nlm}$ are the adiabatic wave functions. In the ARSENY code, they are expressed through the spherical functions in the fixed coordinate system with the aid of the Wigner $d$-function [13, 170].

**7.2.3 Results of calculation and discussion.** The ARSENY code utilized for numerical calculations is based on the theoretical approach described by Solov'ev [171]. This approach is valid when the energy of the system $\varepsilon = \mu v^2/2$ is much higher than the electron energy of the initial state. This condition determines the lower bound of the collision energy for the reactions under consideration: $E \geqslant 10$ eV/u.

The total cross sections for the charge exchange reactions $\mathrm{Li}^{3+} + \mathrm{H(D,T)(1s)}$, calculated using the ARSENY code, are displayed in Fig. 21b. The same cross section calculated without taking into account the rotational interaction $P^{\mathrm{R}}$ is also shown. As is seen from the figure, the rotational interaction starts to contribute to the cross sections for collision energies below 10 keV/u. This contribution increases as the energy decreases, and it is larger for the heavier isotope. A comparison with experimental data [199] shows a good agreement with the calculated results for the reaction with the H target. With a further energy decrease, the influence of the rotational interaction diminishes. For energies below 60 eV/u, the cross section corresponding to the reaction with H is only determined by the radial coupling, while the main contribution to the D and T cross sections is still due to the rotational interaction. This can be explained by the fact that, for the collision of the $\mathrm{Li}^{3+}$ ion with the hydrogen atom, the internuclear distance $R_t$ (the turning point), which satisfies the condition [189]

$$\varepsilon = \frac{(L + 1/2)^2}{2\mu R_t^2} + \frac{Z_1 Z_2}{R_t}\,, \tag{100}$$

is larger than $R_{\max}$ (94), and for these collision energies the $\mathrm{Li}^{3+}$ ion does not reach the region where rotational coupling emerges.

The probability of electron capture on the $n = 3$ level of the $\mathrm{Li}^{2+}$ ion [resonance channel of reaction (87)] averaged over the Stueckelberg oscillations is demonstrated in Fig. 21c, d as a function of the impact parameter. These probabilities correspond to the collision energies $E_1 = 0.04$ keV/u and $E_2 = 0.1$ keV/u denoted in Fig. 21b. At the $E_1$ energy, the charge exchange probabilities for the D and T targets are defined by the probabilities of rotational transitions $3\mathrm{d}_\sigma - 3\mathrm{d}_\pi$, while for the H target the probability is close to zero and coincides with the probability calculated excluding the rotational interaction. It can be seen from the figure that for the tritium target the rotational coupling affects the charge-exchange cross sections in a wider range of impact parameters than in collisions with a deuterium target. At the energy $E_2$, the projectile in collisions with the hydrogen target enters the region of rotational coupling as well, and all three probabilities are determined by the rotational transitions.

The reverse process, namely

$$\mathrm{H(D,T)}^+ + \mathrm{C}(1\mathrm{s}^2 2\mathrm{s}^2 2\mathrm{p}^2) \to \mathrm{H(D,T)}(nl) + \mathrm{C}^+(1\mathrm{s}^2 2\mathrm{s}^2 2\mathrm{p})\,, \tag{101}$$

was studied in paper [197]. The cross sections and the transition probabilities for this reaction were calculated with an effective charge $Z_{\mathrm{eff}} = 1.86$ for the initial 2p state of the

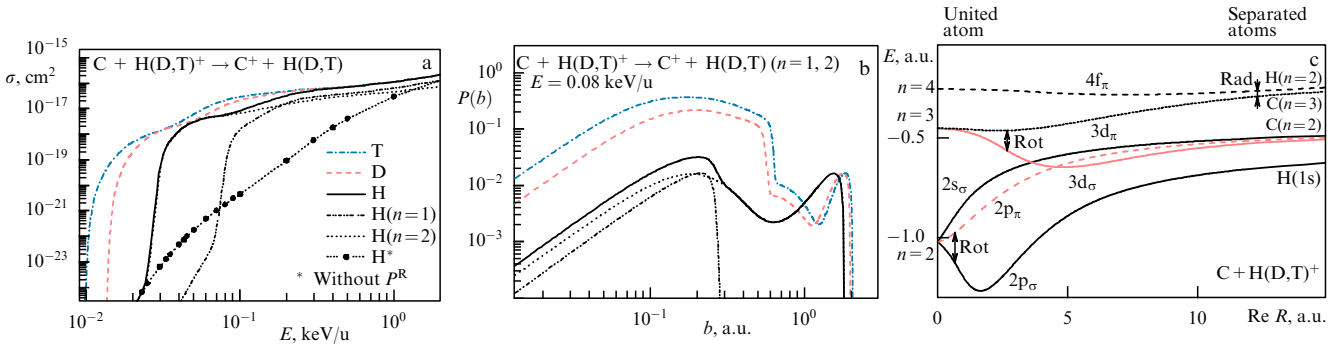


**Figure 22.** (Color online.) (a) The total charge-exchange cross section as a function of collision energy, calculated with and without regard for rotational interaction $P^{\mathrm{R}}$. (b) Probability of the transition as a function of the impact parameter. (c) The potential curves describing the charge exchange process $\mathrm{H}^+ + \mathrm{C}(1s^2 2s^2 2p^2)$ as a function of the internuclear distance.

electron in a C atom. The CDW code, based on the Coulomb distorted wave approximation, was used in paper [54] for the calculation of the effective charge. The results of the calculation are given in Fig. 22. In this case, two reaction channels with final states of H (D, T) ($n = 1$) and H (D, T) ($n = 2$) make the main contribution to the total cross section: $n = 2$ for the lower, and $n = 1$ for the higher collision energies at which the rotational interaction plays the main role. This feature manifests itself in the nonmonotonic behavior of the total cross section.

The contribution from each channel to the total cross section for the $\mathrm{H}^+$ ion is illustrated in Fig. 22a. Electronic energies of the states which contribute to the isotope effect in charge exchange process (101) are shown in Fig. 22c. The initial 2p0 and 2p1 states of the electron in a C atom correspond to $3d_\sigma$ and $2p_\pi$ states in the united atom limit. The transition from the initial state C(2p1) to the final state H(D, T)(1s0) ($2p_\sigma$ in the unified atom limit) is accounted for by the rotational transition $2p_\pi - 2p_\sigma$. Rotational transition $3d_\sigma - 3d_\pi$ and the subsequent radial transition $3d_\pi - 4f_\pi$ occurring at $R = 13.7$ a.u. are responsible for the transition to the final H(D, T) ($n = 2$) state [the $4f_\pi$ state corresponds to H(D, T)(2p1) in the limit of separated atoms].

Figure 22b displays the dependence of the charge exchange probability on the impact parameter at collision energy $E = 0.08$ keV/u. At this energy, all three ions reach the region of rotational interaction. The contributions of the $n = 1$ and $n = 2$ channels are shown for the $\mathrm{H}^+$ ion.

The total cross sections for the charge exchange reaction

$$\mathrm{W}^+(6s) + \mathrm{H}(\mathrm{D},\mathrm{T})(1s) \to \mathrm{W}(6s^2) + \mathrm{H}(\mathrm{D},\mathrm{T})^+ \qquad (102)$$

are plotted in Fig. 23. At present, this process is of great interest, since tungsten ($Z = 74$) is selected as a key material of plasma facing components in the ITER tokamak, where tritium plasma is planned to be ignited. Process (102) plays an important role in the charge distribution, radiative cooling, and particle transport in low-temperature plasmas (edge and divertor plasmas). A comparison of the calculated data with the experimental findings yields a good agreement for the reaction with a hydrogen target [198].

Analyzing the data obtained, one can conclude that the isotope effect is pronounced if the charge exchange reaction has a resonance or quasiresonance channel — that is, if the energies of the initial and final states of the electrons are exactly equal or differ by a small value. In this case, the rotational interaction at collision energies satisfying the

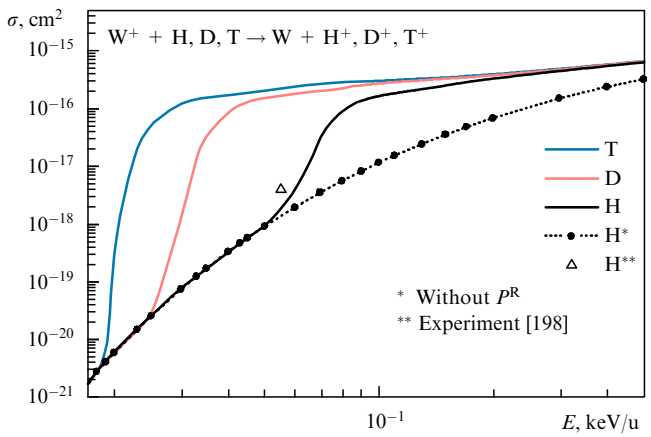


**Figure 23.** (Color online.) Total charge-exchange cross section as a function of collision energy calculated with and without regard for rotational interaction $P^{\mathrm{R}}$ for the reaction $\mathrm{W}^+(6s) + \mathrm{H}(\mathrm{D},\mathrm{T})(1s)$.

condition $R_t < R_{max}$ [equations (100) and (94)] dominates the radial one, rotational transitions make the main contribution to the total charge-exchange cross section, and the isotope effect is observed. The significant difference in the charge-exchange cross sections for the reactions with H, D, and T atoms (several orders of magnitude) indicates the necessity of accounting for the isotope effect in the modeling of edge and divertor plasmas in fusion machines utilizing hydrogen isotopes.

## 8. Conclusions

In the last few years, fast development of accelerating technology and plasma beam diagnostic methods increase the interest in theoretical physics of atomic collisions involving heavy many-electron atoms and ions, especially in the effective cross sections of charge-changing processes: electron capture and electron loss. New experimental data on the cross sections obtained at modern powerful accelerators have led to construction of new theoretical models and creation of corresponding computer codes. The main peculiarity of these many-electron atomic systems is the effect of inner-shell electrons: in many cases they play a key role and a contribution of the outer-shell electrons becomes negligibly small. The influence of inner-shell electrons leads to a change in the scaling laws for the collision cross sections as a function of atomic parameters. A part of this review is just devoted to

the problems mentioned above, although a lot of them are still to be solved in the future. There are some unresolved experimental problems as well, for example, measurements of the electron-loss cross sections at relativistic energies $E > 200$ MeV/u where experimental data are still absent. In this respect, the International FAIR project, started in 2011, seems to be very perspective: according to it heavy ions like $U^{28+}$ are planned to be accelerated up to relativistic energies $\sim 10$ GeV/u for further investigation of their spectroscopic and collisional properties.

Another interesting aspect of the modern physics of atomic collisions, considered in this review, centers around the influence of the isotope effect on the cross sections of resonant and quasiresonant electron capture by low-energy ions colliding with hydrogen isotopes H, D, and T. Most probably, these processes will be of a high interest for specialists studying D – T plasmas due to two main reasons. First, these processes exhibit the dominant mechanisms for creating in a plasma the impurity ions in excited states, radiative decay of which is utilized for plasma diagnostics. Second, a high interest is now related to W ($Z = 74$) atoms and ions because tungsten is considered as the most perspective element for making walls and diverter in plasma devices with magnetic confinement, where the interaction of W atoms and ions with hydrogen and its isotopes play an important role. It should be noted that the common scaling laws for electron-capture cross sections are not valid for low-energy collisions with hydrogen isotopes, and that the influence of the isotope effect on the resonant and quasi-resonant electron-capture cross sections is extremely strong: the cross sections for the reactions with different isotopes may differ by more than three orders of magnitude; therefore, investigation of these processes requires a special attention.

The authors are grateful to V S Lebedev and A A Narits for the fruitful discussions of and valuable remarks on the manuscript.

## References


1. Bates D R *Atomic and Molecular Processes* (New York: Academic Press, 1962) [Translated into Russian (Moscow: Mir, 1964)]
2. Bethe H A *Intermediate Quantum Mechanics* (New York: W.A. Benjamin, 1964)
3. Mott N F, Massey H S W *The Theory of Atomic Collisions* (Oxford: Clarendon Press, 1965) [Translated into Russian (Moscow: Mir, 1969)]
4. Presnyakov L P *Sov. Phys. Usp.* **19** 387 (1976) [*Usp. Fiz. Nauk* **119** 49 (1976)]
5. Sobelman I I, Vainshtein L A, Yukov E A *Excitation of Atoms and Broadening of Spectral Lines* (Berlin: Springer-Verlag, 1981) [Translated from Russian: Vainshtein L A, Sobelman I I, Yukov E A *Vozbuzhdenie Atomov i Ushirenie Spektral'nykh Linii* (Moscow: Nauka, 1979)]
6. Smirnov B M *Sov. Phys. Usp.* **24** 251 (1981) [*Usp. Fiz. Nauk* **133** 569 (1981)]
7. Janev R K, Presnyakov L P *Phys. Rep.* **70** 1 (1981)
8. Janev R K, Presnyakov L P, Shevelko V P *Physics of Highly Charged Ions* (Springer Series in Electrophysics, Vol. 13) (Berlin: Springer-Verlag, 1985); Presnyakov L P, Shevelko V P, Janev R K *Elementarnye Protsessy s Uchastiem Mnogozaryadnykh Ionov* (Moscow: Energoatomizdat, 1986)
9. Shevelko V P, Vainshtein L A *Atomic Physics for Hot Plasmas* (Bristol: IOP Publ., 1993); Vainshtein L A, Shevelko V P *Struktura i Kharakteristiki Ionov v Goryachei Plazme* (Moscow: Nauka, 1986)
10. Janev R K et al. *Elementary Processes in Hydrogen-Helium Plasmas* (Springer Series on Atoms + Plasmas, Vol. 4) (Berlin: Springer-Verlag, 1987)
11. Nikitin E E, Smirnov B M *Atomno-Molekulyarnye Protsessy v Zadachakh s Resheniyami* (Atomic-Molecular Processes in Problems with Solutions) (Moscow: Nauka, 1988)
12. Parilis E S et al. *Ozhe-protsessy pri Atomnykh Stolknoveniyakh* (Auger Processes in Atomic Collisions) (Exec. Ed. O B Firsov) (Tashkent: FAN, 1989)
13. Solov'ev E A *Sov. Phys. Usp.* **32** 228 (1989) [*Usp. Fiz. Nauk* **157** 437 (1989)]
14. Nikitin E E, Smirnov B M *Medlennye Atomnye Stolknoveniya* (Slow Atomic Collisions) (Moscow: Energoatomizdat, 1990)
15. Fritsch W, Lin C D *Phys. Rep.* **202** 1 (1991)
16. Bransden B H, McDowell M R C *Charge Exchange and the Theory of Ion-Atom Collisions* (Oxford: Clarendon Press, 1992)
17. Janev R K (Ed.) *Atomic and Molecular Processes in Fusion Edge Plasmas* (New York: Plenum Press, 1995)
18. Lebedev V S, Beigman I L *Physics of Highly Excited Atoms and Ions* (Springer Series on Atoms + Plasmas, Vol. 22) (Berlin: Springer-Verlag, 1998)
19. Beyer H F, Shevelko V P (Eds) *Atomic Physics with Heavy Ions* (Springer Series on Atoms + Plasmas, Vol. 26) (Berlin: Springer, 1999)
20. Smirnov B M *Phys. Usp.* **44** 221 (2001) [*Usp. Fiz. Nauk* **171** 233 (2001)]
21. Stolterfoht N, DuBois R D, Rivarola R D *Electron Emission in Heavy–Ion–Atom Collisions* (Springer Series on Atoms + Plasmas, Vol. 20) (Berlin: Springer, 1997)
22. Beyer H F, Shevelko V P *Introduction to the Physics of Highly Charged Ions* (Bristol: IOP Publ., 2003)
23. Currell F J (Ed.) *The Physics of Multiply and Highly Charged Ions* (Dordrecht: Kluwer Acad. Publ., 2003)
24. Shevelko V, Tawara H (Eds) *Atomic Processes in Basic and Applied Physics* (Springer Ser. on Atomic, Optical, and Plasma Physics, Vol. 68) (Berlin: Springer-Verlag, 2012)
25. Sharkov B Yu *Nucl. Instrum. Meth. Phys. Res. A* **577** 14 (2007)
26. Logan B G, Perkins L J, Barnard J J *Phys. Plasmas* **15** 072701 (2008)
27. Geissel H et al. *Nucl. Instrum. Meth. Phys. Res. B* **195** 3 (2002)
28. Hickok R L *Rev. Sci. Instrum.* **38** 142 (1967)
29. Geissel H, Münzenberg G, Riisager K *Annu. Rev. Nucl. Part. Sci.* **45** 163 (1995)
30. Mazing M A et al. *Phys. Rev. A* **32** 3695 (1985)
31. Fortov V E, Hoffmann D H H, Sharkov B Yu *Phys. Usp.* **51** 109 (2008) [*Usp. Fiz. Nauk* **178** 113 (2008)]
32. Dennerl K *Space Sci. Rev.* **157** 57 (2010)
33. Amaldi U, Kraft G *Europhys. News* **36** 114 (2005)
34. Nikoghosyan A et al. *Int. J. Radiat. Oncology Biol. Phys.* **58** 89 (2004)
35. FAIR Baseline Technical Report (2006), http://www.fair-center.eu/for-users/publications/fair-publications.html
36. Betz H-D *Rev. Mod. Phys.* **44** 465 (1972)
37. Isler R C *Plasma Phys. Control. Fusion* **36** 171 (1994)
38. Cantrell C D, Scully M O, in *Progress in Lasers and Laser Fusion* (Studies in the Natural Sciences, Vol. 8, Eds A Perlmutter, S M Widmayer) (New York: Plenum Press, 1975) p. 147
39. Rocca J J *Rev. Sci. Instrum.* **70** 3799 (1999)
40. Mokler P H, Stöhlker Th *Adv. Atom. Mol. Opt. Phys.* **37** 297 (1996)
41. Kaminskii A K, Vasil'ev A A *Phys. Part. Nucl.* **29** 201 (1998) [*Fiz. Elem. Chastits At. Yadra* **29** 489 (1998)]
42. Omet C et al. *New J. Phys.* **8** 284 (2006)
43. Eichler J, Stöhlker Th *Phys. Rep.* **439** 1 (2007)
44. Erb W, GSI Report P-7-78 (Darmstadt: GSI, 1978)
45. Perumal A N et al. *Nucl. Instrum. Meth. Phys. Res. B* **227** 251 (2005)
46. Faddeev L D *Tr. Mat. Inst. Akad. Nauk* **69** 3 (1963)
47. Presnyakov L P, Ulantsev A D *Sov. J. Quantum Electron.* **4** 1320 (1974) [*Kvantovaya Elektron.* **1** 2377 (1974)]
48. Presnyakov L P, Uskov D B, Janev R K *Sov. Phys. JETP* **56** 525 (1982) [*Zh. Eksp. Teor. Fiz.* **83** 933 (1982)]
49. Wu Y et al. *Phys. Rev. A* **84** 022711 (2011)
50. Nikulin V K, Guschina N A *Tech. Phys.* **52** 148 (2007) [*Zh. Tekh. Fiz.* **77** (2) 8 (2007)]
51. Chibisov M I *JETP Lett.* **24** 46 (1976) [*Pis'ma Zh. Eksp. Teor. Fiz.* **24** 56 (1976)]
52. Olson R E, Salop A *Phys. Rev. A* **14** 579 (1976)

53. Bárány A, Setterlind C J *Nucl. Instrum. Meth. Phys. Res. B* **98** 184 (1995)
54. Ryufuku H, Watanabe T *Phys. Rev. A* **20** 1828 (1979)
55. Belkić Dž, Mančev I, Hanssen J *Rev. Mod. Phys.* **80** 249 (2008)
56. Tupitsyn I I et al. *Phys. Rev. A* **82** 042701 (2010)
57. Thwaites D I *Nucl. Instrum. Meth. Phys. Res. B* **12** 84 (1985)
58. Belkić Dž, Gayet R, Salin A *Comput. Phys. Commun.* **23** 153 (1981)
59. Belkić Dž, Gayet R, Salin A *Comput. Phys. Commun.* **32** 385 (1984)
60. Olson R E, Ullrich J, Schmidt-Böcking H *Phys. Rev. A* **39** 5572 (1989)
61. Stohlker T et al. *J. Phys. B At. Mol. Opt. Phys.* **25** 4527 (1992)
62. Perez J A, Olson R E, Beiersdorfer P *J. Phys. B At. Mol. Opt. Phys.* **34** 3063 (2001)
63. Blank I et al. *Phys. Rev. A* **85** 022712 (2012)
64. Eichler J, Chan F T *Phys. Rev. A* **20** 104 (1979)
65. Shevelko V P et al. *J. Phys. B At. Mol. Opt. Phys.* **37** 201 (2004)
66. Schlachter A S et al. *Phys. Rev. A* **27** 3372 (1983)
67. Shevelko V P et al. *Nucl. Instrum. Meth. Phys. Res. B* **268** 2611 (2010)
68. Olson R E et al. *J. Phys. B At. Mol. Opt. Phys.* **35** 1893 (2002)
69. Alonso J, Gould H *Phys. Rev. A* **26** 1134 (1982)
70. Cocke C L, Olson R E *Phys. Rep.* **205** 153 (1991)
71. Knudsen H, Haugen H K, Hvelplund P *Phys. Rev. A* **24** 2287 (1981)
72. Bates D R, Griffing G W *Proc. Phys. Soc. A* **68** 90 (1955)
73. Matveev V I, Sidorov D B *Tech. Phys.* **52** 839 (2007) [*Zh. Tekh. Fiz.* **77** (7) 18 (2007)]
74. Shevelko V P, Litsarev M S, Tawara H *J. Phys. B At. Mol. Opt. Phys.* **41** 115204 (2008)
75. Shevelko V P, Tolstikhina I Yu, Stöhlker Th *Nucl. Instrum. Meth. Phys. Res. B* **184** 295 (2001)
76. Shevelko V P et al. *Nucl. Instrum. Meth. Phys. Res. B* **269** 1455 (2011)
77. Carlson T A et al. *Atom. Data Nucl. Data Tabl.* **2** 63 (1970)
78. Desclaux J P *Atom. Data Nucl. Data Tabl.* **12** 311 (1973)
79. Zschornack G, Musiol G, Wagner W "Dirac–Fock–Slater X-ray energy shifts and electron binding energy changes for all ion ground states in elements up to uranium", Preprint ZfK-574 (Rossendorf bei Dresden: Zentralinstitut für Kernforschung, 1986)
80. Rashid K, Saadi M Z, Yasin M *Atom. Data Nucl. Data Tabl.* **40** 365 (1988)
81. Gröbner O et al. (GSI/CERN Collab.) (Darmstadt: GSI, 1993), unpublished
82. Franzke B *IEEE Trans. Nucl. Sci.* **28** 2116 (1981)
83. DuBois R D et al. *Phys. Rev. A* **70** 032712 (2004)
84. Müller C, Voitkiv A B, Grün N *Phys. Rev. A* **66** 012716 (2002)
85. Shevelko V P et al. *Nucl. Instrum. Meth. Phys. Res. B* **278** 63 (2012)
86. Eichler J, Meyerhof W E *Relativistic Atomic Collisions* (San Diego: Academic Press, 1995)
87. Voitkiv A B *Phys. Rep.* **392** 191 (2004)
88. Voitkiv A, Ullrich J *Relativistic Collisions of Structured Atomic Particles* (Springer Series on Atomic, Optical and Plasma Physics, Vol. 49) (Berlin: Springer, 2008)
89. Voitkiv A B, Najjari B, Surzhykov A *J. Phys. B At. Mol. Opt. Phys.* **41** 111001 (2008)
90. Najjari B, Surzhykov A, Voitkiv A B *Phys. Rev. A* **77** 042714 (2008)
91. Beigman I L, Tolstikhina I Yu, Shevelko V P *Tech. Phys.* **53** 547 (2008) [*Zh. Tekh. Fiz.* **78** (5) 15 (2008)]
92. Andreev S N et al. *Bull. Lebedev Phys. Inst.* **35** 89 (2008) [*Kratk. Soobshch. Fiz. FIAN* **35** (3) 39 (2008)]
93. Bethe H, in *Handbuch der Physik* Vol. 34 (Berlin: Springer, 1933) p. 273
94. Anholt R et al. *Phys. Rev. A* **32** 3302 (1985)
95. Davidovic D M et al. *J. Phys. B At. Mol. Phys.* **11** 847 (1978)
96. Jackson J D *Classical Electrodynamics* (New York: Wiley, 1975)
97. Bertulani C A, Baur G *Phys. Rep.* **163** 299 (1988)
98. Baur G et al. *Phys. Rev. A* **80** 012713 (2009)
99. Tolstikhina I Yu, Shevelko V P *JETP Lett.* **94** 152 (2011) [*Pis'ma Zh. Eksp. Teor. Fiz.* **94** 157 (2011)]
100. Olson R E et al. *J. Phys. B At. Mol. Opt. Phys.* **37** 4539 (2004)
101. Bohr N *Philos. Mag.* **30** 581 (1915)
102. Cocke C L *Phys. Rev. A* **20** 749 (1979)
103. Shevelko V P et al. *J. Phys. B At. Mol. Opt. Phys.* **43** 215202 (2010)
104. Salvat F et al. *Phys. Rev. A* **36** 467 (1987)
105. Song M-Y et al. *Nucl. Instrum. Meth. Phys. Res. B* **267** 2369 (2009)
106. Olson R E et al. *Nucl. Instrum. Meth. Phys. Res. A* **544** 333 (2005)
107. Crandall D H et al. *Phys. Rev. Lett.* **36** 858 (1976)
108. Klinger H, Muller A, Salzborn E *J. Phys. B At. Mol. Phys.* **8** 230 (1975)
109. Müller A, Salzborn E *Phys. Lett. A* **62** 391 (1977)
110. Crandall D H, Phaneuf R A, Meyer F W *Phys. Rev. A* **22** 379 (1980)
111. Tawara H et al. *J. Phys. B At. Mol. Phys.* **18** 337 (1985)
112. Müller A et al. *Phys. Rev. A* **33** 3010 (1986)
113. Selberg N, Biedermann C, Cederquist H *Phys. Rev. A* **54** 4127 (1996)
114. Selberg N, Biedermann C, Cederquist H *Phys. Rev. A* **56** 4623 (1997)
115. Suzuki K, Okuno K, Kobayashi N *Phys. Scripta* **1997** (T73) 172 (1997)
116. Kimura M et al. *J. Phys. B At. Mol. Opt. Phys.* **28** L643 (1995)
117. Nakamura N et al. *J. Phys. B At. Mol. Opt. Phys.* **28** 2959 (1995)
118. Sakaue H A et al. *J. Phys. B At. Mol. Opt. Phys.* **37** 403 (2004)
119. Bräuning H et al. *Phys. Rev. Lett.* **91** 168301 (2003)
120. Zettergren H et al. *Eur. Phys. J. D* **38** 299 (2006)
121. Wethekam S et al. *Phys. Rev. B* **81** 121416(R) (2010)
122. Narits A A *J. Phys. B At. Mol. Opt. Phys.* **41** 135102 (2008)
123. Bohr N, Lindhard J *Danske Videnskab. Selskab. Math.-Fys. Medd.* **28** (7) (1954)
124. Bárány A et al. *Nucl. Instrum. Meth. Phys. Res. B* **9** 397 (1985)
125. Niehaus A *J. Phys. B At. Mol. Phys.* **19** 2925 (1986)
126. Harel C, Jouin H *J. Phys. B At. Mol. Opt. Phys.* **25** 221 (1992)
127. Chen Z, Shingal R, Lin C D *J. Phys. B At. Mol. Opt. Phys.* **24** 4215 (1991)
128. Hansen J P, Taulbjerg K *Phys. Rev. A* **45** R4214 (1992)
129. Nikulin V K, Guschina N A *Phys. Scripta* **1997** (T71) 134 (1997)
130. Sidorovich V A, Nikolaev V S, McGuire J H *Phys. Rev. A* **31** 2193 (1985)
131. Cederquist H et al. *Phys. Rev. A* **61** 022712 (2000)
132. Watson R L et al. *Phys. Rev. A* **67** 022706 (2003)
133. Mueller D et al. *Phys. Plasmas* **8** 1753 (2001)
134. Russek A, Meli J *Physica* **46** 222 (1970)
135. DuBois R D et al. *Phys. Rev. A* **68** 042701 (2003)
136. Santos À C F, DuBois R D *Phys. Rev. A* **69** 042709 (2004)
137. Rost J M, Pattard T *Phys. Rev. A* **55** R5 (1997)
138. Weber G et al. *Phys. Rev. ST Accel. Beams* **12** 084201 (2009)
139. Lassen N O *Danske Videnskab. Selskab. Mat.-Fys. Medd.* **26** (5) (1951)
140. Lassen N O *Danske Videnskab. Selskab. Mat.-Fys. Medd.* **26** (12) (1951)
141. Geissel H et al. *Phys. Lett. A* **99** 77 (1983)
142. Betz H D, Grodzins L *Phys. Rev. Lett.* **25** 211 (1970)
143. Miyoshi T et al. *Nucl. Instrum. Meth. Phys. Res. B* **258** 329 (2007)
144. Fettouhi A et al. *Nucl. Instrum. Meth. Phys. Res. B* **245** 32 (2006)
145. Ogawa H et al. *Phys. Rev. A* **75** 020703(R) (2007)
146. Eisenbarth S et al. *Laser Part. Beams* **25** 601 (2007)
147. Ryding G, Betz H D, Wittkower A *Phys. Rev. Lett.* **24** 123 (1970)
148. Woods C J et al. *J. Phys. B At. Mol. Phys.* **17** 867 (1984)
149. Shevelko V P et al. *J. Phys. B At. Mol. Opt. Phys.* **38** 2675 (2005)
150. Klein O, Rosseland S *Z. Phys.* **4** 46 (1921)
151. Wahl H et al. *Kratk. Soobshch. Fiz. FIAN* (8) 28 (2001)
152. Krämer A et al., in *Proc. of the 8th European Particle Accelerator Conf., EPAC 2002, Paris, 3–7 June 2002* (Geneva: EPS-IGA, CERN, 2002) p. 2547; http://accelconf.web. cern.ch/accelconf/e02/PAPERS/WEPLE116.pdf
153. Spiller P et al., GSI Scientific Report 2010 (Darmstadt: GSI, 2011) p. 270
154. Born M, Oppenheimer R *Ann. Physik* **84** 457 (1927)
155. Born M, Fock V *Z. Phys.* **51** 165 (1928)
156. Landau L D *Phys. Z. Sowjetunion* **1** 88 (1932)
157. Dykhne A M *Sov. Phys. JETP* **14** 941 (1962) [*Zh. Eksp. Teor. Fiz.* **41** 1324 (1961)]
158. Zener C *Proc. R. Soc. Lond. A* **137** 696 (1932)
159. Stueckelberg E C G *Helv. Phys. Acta* **5** 369 (1932)
160. Smirnov B M *Atomnye Stolknoveniya i Elementarnye Protsessy v Plazme* (Atomic Collisions and Elementary Processes in Plasmas) (Moscow: Nauka, 1968)
161. Nikitin E E *Theory of Elementary Atomic and Molecular Processes in Gases* (Oxford: Clarendon Press, 1974) [Translated from Russian:

*Teoriya Elementarnykh Atomno-Molekulyarnykh Protsessov v Gazakh* (Moscow: Khimiya, 1970)]
162. Nikitin E E *Teoriya Elementarnykh Atomno-molekulyarnykh Reaktsii* Vols 1, 2 (Theory of Atomic-molecular Reactions) (Novosibirsk: Izd. Novosibirsk. Univ., 1970, 1974)
163. Nikitin E E, Smirnov B M *Sov. Phys. Usp.* **21** 95 (1978) [*Usp. Fiz. Nauk* **124** 201 (1978)]
164. Nikitin E E, Umanskii S Ya *Theory of Slow Atomic Collisions* (Berlin: Springer-Verlag, 1984) [Translated from Russian: *Neadiabaticheskie Perekhody pri Medlennykh Atomnykh Stolknoveniyakh* (Moscow: Atomizdat, 1979)]
165. Demkov Yu N *Sov. Phys. JETP* **18** 138 (1964) [*Zh. Eksp. Teor. Fiz.* **45** 195 (1963)]
166. Nikitin E E *Opt. Spectrosc.* **13** 431 (1962) [*Opt. Spektrosk.* **13** 761 (1962)]
167. Osherov V I *Sov. Phys. JETP* **22** 804 (1965) [*Zh. Eksp. Teor. Fiz.* **49** 1157 (1965)]
168. Demkov Yu N *Sov. Phys. Dokl.* **11** (8) 138 (1966) [*Dokl. Akad. Nauk SSSR* **166** 1076 (1966)]
169. Demkov Yu N, Osherov V I *Sov. Phys. JETP* **26** 916 (1968) [*Zh. Eksp. Teor. Fiz.* **53** 1589 (1967)]
170. Solov'ev E A *J. Phys. B At. Mol. Opt. Phys.* **38** R153 (2005)
171. Solov'ev E A, in *Workshop on Hidden Crossings in Ion–Atom Collisions and in Other Nonadiabatic Transitions* (Cambridge: Harvard Smithsonian Centre for Astrophysics, 1991)
172. Komarov I V, Ponomarev L I, Slavyanov S Yu *Sferoidal'nye i Kulonovskie Sferoidal'nye Funktsii* (Spheroidal and Coulomb Spheroidal Functions) (Moscow: Nauka, 1976)
173. Esry B D et al. *J. Phys. B At. Mol. Opt. Phys.* **26** 1579 (1993)
174. Blanco S A, Falcon C A, Piacentini R D *J. Phys. B At. Mol. Phys.* **19** 3945 (1986)
175. Krstić P S et al. *Phys. Rev. A* **70** 042711 (2004)
176. Toshima N, Tawara H, NIFS-DATA-026 (Nagoya: NIFS, 1995)
177. Zhang P et al. *Phys. Chem. Chem. Phys.* **13** 19026 (2011)
178. Chen C Y et al. *J. Phys. B At. Mol. Opt. Phys.* **34** 469 (2001)
179. Deumens E et al. *Rev. Mod. Phys.* **66** 917 (1994)
180. Igarashi A, Lin C D *Phys. Rev. Lett.* **83** 4041 (1999)
181. Kado S et al., in *Proc. of the 19th Intern. Conf. on Plasma-Surface Interaction, San Diego, May 24 – 28, 2010*
182. Kado S et al. *J. Plasma Fusion Res.* **81** 810 (2005)
183. Firsov O B *Zh. Eksp. Teor. Fiz.* **21** 1001 (1951)
184. Matveenko A V, Ponomarev L I *Sov. Phys. JETP* **41** 456 (1975) [*Zh. Eksp. Teor. Fiz.* **68** 920 (1975)]
185. Hunter G, Kuriyan M *Proc. R. Soc. Lond. A* **353** 575 (1977)
186. Tolstikhina I Yu, Kato D *Phys. Rev. A* **82** 032707 (2010)
187. Rosen N, Zener C *Phys. Rev.* **40** 502 (1932)
188. Ovchinnikov S Yu, Solov'ev E A *Sov. Phys. JETP* **63** 538 (1986) [*Zh. Eksp. Teor. Fiz.* **90** 921 (1986)]
189. Landau L D, Lifshitz E M *Quantum Mechanics: Non-Relativistic Theory* (Oxford: Pergamon Press, 1977) [Translated from Russian: *Kvantovaya Mekhanika. Nerelyativistskaya Teoriya* (Moscow: Nauka, 1989)]
190. Macek J H, Krstić P S, Ovchinnikov S Yu *Phys. Rev. Lett.* **93** 183203 (2004)
191. Ostrovsky V N *Phys. Rev. A* **61** 032505 (2000)
192. Tolstikhin O I, Namba C *Phys. Rev. A* **60** 5111 (1999)
193. Stolterfoht N et al. *Phys. Rev. Lett.* **99** 103201 (2007)
194. Grozdanov T P, Solov'ev E A *Phys. Rev. A* **42** 2703 (1990)
195. Stolterfoht N et al. *Phys. Rev. A* **81** 052704 (2010)
196. Cabrera-Trujillo R et al. *Phys. Rev. A* **83** 012715 (2011)
197. Tolstikhina I Yu, Kato D, Shevelko V P *Phys. Rev. A* **84** 012706 (2011)
198. Tolstikhina I Yu et al. *J. Phys. B At. Mol. Opt. Phys.* **45** 145201 (2012)
199. Seim W et al. *J. Phys. B At. Mol. Phys.* **14** 3475 (1981)